Atmos. Chem. Phys., 12, 11951–11974, 2012
www.atmos-chem-phys.net/12/11951/2012/
doi:10.5194/acp-12-11951-2012

Atmospheric Chemistry and Physics

Radical budget analysis in a suburban European site during the MEGAPOLI summer field campaign

V. Michoud[1], A. Kukui[2,10], M. Camredon[1], A. Colomb[3], A. Borbon[1], K. Miet[1], B. Aumont[1], M. Beekmann[1], R. Durand-Jolibois[1], S. Perrier[1,4], P. Zapf[1], G. Siour[1], W. Ait-Helal[1,5,6], N. Locoge[5,6], S. Sauvage[5,6], C. Afif[1,7], V. Gros[8], M. Furger[9], G. Ancellet[2], and J. F. Doussin[1]

[1]LISA, UMR-CNRS 7583, Université Paris Est Créteil (UPEC), Université Paris Diderot (UPD), Institut Pierre Simon Laplace (IPSL), Créteil, France
[2]LATMOS, UMR-CNRS 8190, Université de Versailles Saint Quentin, Université Pierre et Marie Curie, Guyancourt, France
[3]LaMP, UMR-CNRS 6016, Clermont Université, Université Blaise Pascal, Aubière, France
[4]ISA, UMR-CNRS 5280, Université Lyon 1, ENS-Lyon, Villeurbanne, France
[5]Université Lille Nord de France, Lille, France
[6]Department of Chemistry and Environment, Ecole des Mines de Douai, Douai, France
[7]Centre d'Analyses et de Recherche, Faculty of sciences, Université Saint Joseph, Beirut, Lebanon
[8]LSCE, Université de Versailles Saint Quentin en Yvelines, CEA, CNRS, Gif sur Yvette, France
[9]Laboratory of Atmospheric Chemistry, Paul Scherrer Institut, Villigen, Switzerland
[10]LPC2E, UMR-CNRS 6115, Orléans, France

Correspondence to: J. F. Doussin (jean-francois.doussin@lisa.u-pec.fr)

Received: 14 June 2012 – Published in Atmos. Chem. Phys. Discuss.: 26 June 2012
Revised: 8 October 2012 – Accepted: 12 November 2012 – Published: 17 December 2012

Abstract. Chemical Ionisation Mass Spectrometer measurements of hydroxyl radical (OH) and the sum of hydroperoxy and organic peroxy (HO_2+RO_2) radicals were conducted during the MEGAPOLI summer field campaign at the SIRTA observatory near Paris, France, in July 2009. OH and (HO_2+RO_2) showed a typical diurnal variation with averaged daytime maxima values around 5×10^6 and 1.2×10^8 molecule cm^{-3}, respectively. Simultaneously, a large number of ancillary measurements, such as NO_x, O_3, HONO, HCHO and other VOCs were also conducted. These data provide an opportunity to assess our understanding of the radical chemistry in a suburban environment by comparing the radical observations to calculations. First, OH mixing ratios were estimated by a simple Photo Stationary State (PSS) calculation. PSS calculations overestimate the OH mixing ratio by 50 %, especially at NO_x mixing ratios lower than 10 ppb, suggesting that some loss processes were missing in the calculation at low NO_x. Then, a photochemical box model simulation based on the Master Chemical Mechanism (MCM) and constrained by ancillary measurements was run to calculate radical concentrations. Three different modelling procedures were tested, varying the way the unconstrained secondary species were estimated, to cope with the unavoidable lack of their measurements. They led to significant differences in simulated radical concentrations. OH and (HO_2+RO_2) concentrations estimated by two selected model version were compared with measurements. These versions of the model were chosen because they lead, respectively, to the higher and lower simulated radical concentrations and are thus the two extremes versions. The box model showed better results than PSS calculations, with a slight overestimation of 12 % and 5 %, for OH and (HO_2+RO_2) respectively, in average for the reference model, and an overestimation of approximately 20 % for OH and an underestimation for (HO_2+RO_2) for the other selected model version. Thus, we can conclude from our study that OH and (HO_2+RO_2) radical levels agree on average with observations within the uncertainty range. Finally, an analysis of the radical budget, on a daily basis (06:00–18:00 UTC), indicates that HONO photolysis (∼35 %), O_3 photolysis (∼23 %), and aldehydes and ketones photolysis (∼16 % for formaldehyde and 18 % for others) are the main radical initiation pathways. According to the MCM

modelling, the reactions of RO_2 with NO_2 (∼19 %), leading mainly to PAN formation, is a significant termination pathway in addition to the main net loss via reaction of OH with NO_2 (∼50 %).

1 Introduction

The hydroxyl (OH) radical is the main oxidant of the troposphere during daytime (Levy, 1972). It plays an important role in the oxidation of many atmospheric species, leading to the formation of secondary pollutants such as ozone (O_3) and Secondary Organic Aerosols (SOA) through a radical cycle where OH is regenerated. Indeed, OH reaction with organic compounds leads to peroxy radicals (RO_2) formation. These peroxy radicals react with NO to form NO_2 and alkoxy radicals (RO). RO next evolves to the formation of hydroperoxy radical (HO_2) and secondary organic compounds. Finally, HO_2 reacts with NO to form OH and NO_2. The radical interconversion cycles effectively link the OH, HO_2 and RO_2 radicals chemistry and lead to the formation of ozone, as a by-product of NO to NO_2 conversion followed by NO_2 photolysis (Finlayson-Pitts and Pitts, 2000).

A major source of radicals in both clean and polluted atmospheres is the ozone photolysis followed by a rapid reaction between $O(^1D)$ and water vapour. In polluted areas, other radical photolytic sources can also be important for radicals, such as nitrous acid (HONO) (Aumont et al., 2003; Acker et al., 2006; Kleffman, 2007) and formaldehyde (HCHO) or other aldehydes photolysis (Emmerson et al., 2005b). Other non photolytic sources can be important for radical production, such as ozone reactions with alkenes, especially during the night in summer or throughout the day during winter (Donahue et al., 1998; Bey et al., 2001; Kanaya et al., 2007), or reactions of NO_3 radical with unsaturated VOC which lead to peroxy radicals during the night (Salisbury et al., 2001; Geyer et al., 2003). In spite of their key role in the atmospheric oxidizing cycles, radical measurements are not always present in field campaign datasets as their great reactivity and low atmospheric concentration make their monitoring difficult.

During the past decades several campaigns including radical measurements were carried out in various environments (Heard and Pilling, 2003). Most of these experiments took place in rural or remote environments (Mount and Williams, 1997; Eisele et al., 1997; Carslaw et al., 1999b, 2001; Creasey et al., 2001; Tan et al., 2001; Kanaya et al., 2001; Creasey et al., 2002; Holland et al., 2003; Mihelcic et al., 2003; Smith et al., 2006; Ren et al., 2006; Hofzumahaus et al., 2009) but some campaigns with radical measurements were also conducted in urban or sub-urban environments (George et al., 1999; Ren et al., 2003b; Emmerson et al., 2005a, 2007; Kanaya et al., 2007; Dusanter et al., 2009).

The common goal of all these studies was to assess our understanding of the previously described oxidizing cycles under various environmental conditions. The relative contribution of the initiation reaction, the efficiency of the recycling pathways and the importance of various sinks were investigated by comparing the radical measurements with results of simulation using different photochemical models constrained with observations of longer-lived species and environmental parameters. An agreement between the measurements and simulations suggests generally that the radical chemistry is adequately described by a model. At the same time, taking apart possible measurement errors, discrepancies between measurements and model may indicate that significant initiation, termination or recycling processes are not properly accounted in the model and that probably important constraints are missing. Such situation is likely to be encountered in complex environments where radical chemistry should be described with accounting for a detailed mechanism including large number of different species (VOCs, OVOCs, etc).

Applied in both rural and urban environments, this approach has led to various outcomes. While the agreement between measured and modelled HO_x is generally good in urban environments (Martinez et al., 2003; Ren et al., 2003a; Shirley et al., 2006; Kanaya et al., 2007), some studies have shown underestimation of OH measurements by models in forested areas at low NO_x (Tan et al., 2001; Carslaw et al., 2001; Hofzumahaus et al., 2009), suggesting unknown non NO-dependent OH regeneration pathways. Indeed, Hofzumahaus et al. (2009) have found strong underestimation by a factor of 3 to 5 of OH concentrations calculated using the Regional Atmospheric Chemical Mechanism (RACM) (Stockwell et al., 1997), whereas good agreement was found for HO_2 concentrations. This difference for OH can neither be explained by uncertainties nor by measurement interferences. The authors proposed two reactions to explain it, $RO_2+X \rightarrow HO_2$ and $HO_2+X \rightarrow OH$, both of similar rates, as in the case of the corresponding NO reactions. The addition of these reactions with a concentration of 0.85 ppb equivalent NO for X allows the model to reproduce well OH and HO_2 concentrations. However, considering the RO_2 interference in the HO_2 detection channel of the LIF-instrument (Fuchs et al., 2011), Lu et al. (2012) have re-evaluated the dataset and extended the model analysis. They concluded that the need of an additional HO_2 to OH recycling process persists but that the need of an unknown recycling RO_2 to HO_2 to match observed HO_2 has diminished. During Intercontinental Chemical Transport Experiment-A (INTEX-A), Ren et al. (2008) compared the HO_x concentrations obtained with a model developed at the NASA Langley Research Center with airborne measurements. For most of the troposphere, the model agrees well with OH and HO_2 observations, with averaged observed-to-model ratios being respectively 0.95 and 1.28. Nonetheless, underestimation for OH correlated with isoprene levels was found in the planetary boundary layer in forested environments: the observed

to model ratio increased from 1 to 1.5 when isoprene rose from less than 10 ppt to 500 ppt and up to 5 when isoprene exceeded 500 ppt.

On the contrary, many studies in remote or rural environments showed an overestimation of simulated OH concentrations at low NO_x and better agreement at high NO_x (Mount and Williams, 1997; Carslaw et al., 1999a; Mihelcic et al., 2003). Indeed, Mihelcic et al. (2003) found that at high NO_x, during BERLIOZ campaign at about 50 km in the North West of the city-center of Berlin, OH is well reproduced by the MCM with a slight overestimation (10–30 %), whereas at low NO_x OH is overpredicted by a factor comprised between 1.5 and 1.7 and RO_2 is overestimated by a factor of 2 or more on some days. This general model radical overestimation at low NO_x suggests that some radical sinks were missing in the model. Using a MCM constrained box model during the EASE97 campaign which took place on the remote west coast of Ireland, Carslaw et al. (2002) have observed an overestimation of both OH and HO_2 by their model, while a good agreement is found for RO_x over a wide range of conditions. The author improved the model-measurements discrepancies by adding HO_2 loss on aerosol surfaces increasing the mass accommodation coefficient of HO_2 to 1 and constraining HO_2 in the model to measured values. However, these changes could not explain all the differences between model and measurements. According to these authors, these discrepancies occurred because the chemical composition of the air mass was not fully characterized. During the NAMBLEX campaign which was conducted at the same site as EASE97, Sommariva et al. (2006) found good agreement between measured and modelled OH concentrations using MCM, within 25 %. The model generally overestimated HO_2 concentrations by about a factor of 2 or more. Nevertheless, better agreements are found for HO_2 concentrations when adding both halogen monoxides chemistry and uptake of HO_2 on sea-salt particles. Using Regional Atmospheric Chemical Mechanism (RACM), Dusanter et al. (2009) noted that his model consistently overestimated the OH concentrations measured during the Mexico City Metropolitan Area (MCMA) field campaign, when dicarbonyls were not constrained. The authors have also observed an underestimation of HO_x during morning hours. These discrepancies increase with higher benzene and toluene concentrations and thus could be explained by a missing source linked to the poorly characterized aromatics oxidation mechanism under high NO_x conditions in the model. A recent study comparing OH measurements from two different methods: a traditional FAGE and a new chemical removal method, has highlighted that some discrepancies between modelled and measured OH concentrations may come from error in OH measurements (Mao et al., 2012). Indeed, these authors found that the two OH measurements, performed in a forested site, give different results, the new method giving on average 40-50 % of the OH traditional FAGE measurements. Furthermore, OH concentrations measured by the new method agree with modelled OH concentrations, using RACM simulation, while OH concentrations measured by traditional FAGE largely overestimate simulated OH concentrations. The authors explain the difference in OH concentrations measured by the two techniques from an internal OH formation causing interferences in the traditional FAGE technique.

Results from all these studies are still far from leading to a clear picture of the chemical mechanisms that are missing in the models. The uncertainties concern all steps of the radical oxidizing cycle, i.e. initiation, propagation and termination processes which are missing or not well enough estimated in the chemical mechanisms. The present work aims at adding some insight in radical atmospheric chemistry and analysing the radical cycles leading to the oxidation of atmospheric species in the suburban region of Paris Megacity. In the frame of MEGAPOLI (Megacities: Emissions, urban, regional and Global Atmospheric POLlution and climate effects, and Integrated tools for assessment and mitigation) project, a radical closure experiment was performed in the Paris region for the first time. Our study is mainly based on the comparison between observed and calculated radical concentrations as well as on a radical budget analysis using both a simple Photo Stationary State calculation (PSS) and a box model containing the Master Chemical Mechanism (MCM) and constrained with all the species and the parameters measured during MEGAPOLI (RH, temperature, pressure, boundary layer high, $J(O^1D)$, $J(NO_2)$, J(HONO), NO, NO_2, O_3, CO, CH_4, CO_2, HCHO, HONO, PAN and 32 VOC). Furthermore, during this study several modelling procedures have been tested in order to investigate the impact on radical estimation of the way the unconstrained secondary species are calculated.

2 The MEGAPOLI experiment

2.1 The SIRTA suburban observatory

The MEGAPOLI summer campaign took place between the 1 and the 31 July 2009 at several ground sites. This study is built on data collected at the SIRTA ("Site Instrumental de Recherche par Télédétection Atmosphérique") observatory (Haeffelin et al., 2005; Pietras et al., 2007). The SIRTA is a French national atmospheric observatory dedicated to cloud and aerosol research and is located at Palaiseau in "Ecole Polytechnique" area (48.718° N, 2.207° E), 14 km south-west of Paris (France) in a semi-urban environment (Freutel et al., 2012). This site is downwind of Paris under anticyclonic conditions and receives oceanic air masses from west of France the rest of the time (Freutel et al., 2012). The choice of this site was motivated by a possibility to compare the radical chemistry under these different conditions.

2.2 OH and (HO_2+RO_2) measurements

The radicals OH, the sum of hydroperoxy and organic peroxy radicals (HO_2+RO_2) and sulfuric acid (not presented here) have been measured using chemical ionisation mass spectrometry (CIMS) (Eisele and Tanner, 1991; Tanner et al., 1997; Berresheim et al., 2000). Detailed description of the instrument has been presented elsewhere (Kukui et al., 2008). Here we briefly present the measurement technique and essential details about the setup and performance of the system during the MEGAPOLI campaign.

The OH radical is measured by converting sampled OH radicals into H_2SO_4 by addition of SO_2 in a chemical conversion reactor (CCR) in the presence of water vapor and oxygen (Eisele and Tanner, 1991; Tanner et al., 1997; Berresheim et al., 2000). H_2SO_4 is detected by using mass spectrometry as HSO_4^- ion is produced by chemical ionisation with NO_3^- in an ion-molecule reactor following the CCR. To account for the contribution of atmospheric sulfuric acid the chemical conversion is performed using isotopically labelled $^{34}SO_2$ leading to the formation of $H_2^{34}SO_4$. The concentration of (HO_2+RO_2) is measured by converting them into OH radicals via reactions with NO (Reiner et al., 1997), hereafter converted into sulfuric acid. The chemical conversion is terminated by addition of NO_2, used as a radical scavenger, into the CCR (Kukui et al., 2008).

During the MEGAPOLI measurements the instrument was installed in a container with the CCR protruding through an interface cap covered with a Teflon sheet and fixed on the roof of the container. Ambient air is sampled into the CCR at a flow rate of 13 L min^{-1} through a sampling aperture (3 mm diameter) placed 50 cm above the roof (i.e. about 4 m above the ground) creating turbulent flow conditions in the reactor to minimise possible wind speed influence and ensure fast mixing of reactants. The CCR was similar to the one described in Kukui et al. (2008) except that the modified reactor is made of stainless steel and its exit tube is used as one of the electrodes forming ion trajectories in an ion-molecule reactor. The ion-molecule reactor has also been modified to allow addition of a "sheath" flow (Tanner et al., 1997) resulting in a significant reduction of the background signal.

Accounting for the calibration uncertainties and measurement precision, the overall 2σ uncertainty of the 10 min averaged measurements of OH and (HO_2+RO_2) is estimated to be 35 % and 45 %, respectively. The detection limit of 8×10^5molecule cm^{-3} for one 2 min OH point was calculated from the signal statistics in background mode at a signal to noise ratio of 3. More detailed descriptions of the different measurement modes, the instrument calibration, the estimation of measurement precision and the data correction can be found in the Supplement S1.

2.3 Photolysis frequencies measurements

During the MEGAPOLI summer campaign, measurements of $J(NO_2)$ and $J(O^1D)$ were performed using two filterradiometers and measurements of J(HONO) using a spectroradiometer (LI-1800). The $J(NO_2)$ filterradiometer was installed at the top of a 9m mast. It was calibrated at the "Institut für Energie und Klimaforschung" at the Forschungszentrum Jülich GmbH in January 2011. Accounting for the calibration uncertainties and measurement precision, the 2σ uncertainty of the $J(NO_2)$ measurements is estimated to be 20 %.

The $J(O^1D)$ filterradiometer was installed on the same container roof as the CIMS inlet. The two filterradiometers were at a distance of about 10m. The $J(O^1D)$ filterradiometer can not be calibrated. Thus, we compared its measurements with $J(O^1D)$ calculated using the Tropospheric Ultraviolet and Visible (TUV version 5.0) (Madronich et al., 1998; McKenzie et al., 2007) radiation model for clear sky days (http://cprm.acd.ucar.edu/Models/TUV/). The Ozone Column used in these calculations came from data measured in Paris center in a station of the "Système d'Analyse par Observation Zénithale" (SAOZ) network (http://saoz.obs.uvsq.fr/saoz/). With this calculation the best fit between $J(NO_2)$ calculated and measured was found for a surface albedo of 0.1. Since the surface albedo is supposed to be smaller in the UV-B (Webb et al., 2000), we used a surface albedo of 0.05 for $J(O^1D)$ calculation (representative of an albedo in UV-B for a mix surface of grass (0.02) and Tarmac (0.08) (Webb et al., 2000)). With the above assumption about the surface albedo, a good correlation ($R^2>0.99$) found between the calculated and measured $J(O^1D)$ for two clear sky days allows a reasonable estimation of the filterradiometer response factor. However, accounting for the calculation and the measurement uncertainties, the $J(O^1D)$ measurement uncertainty is estimated to be 20 %.

The spectroradiometer (LI-1800), that uses a manual shadower technique to estimate the direct and diffuse radiation (Cotte, 1995), was deployed in order to calculate other photolysis frequencies. This instrument was installed near the ground in the middle of a field, to avoid any effect of building shadows, and was about 20 m away from the two filterradiometers. The LI-1800 spectroradiometer results were scaled with the calibrated data of the $J(NO_2)$ filterradiometer. Only the nitrous acid photolysis frequency (J(HONO)) was measured with this spectroradiometer, uncertainties at lower wavelength being too large. Accounting for the combined uncertainties of LI-1800 and $J(NO_2)$ measurements the J(HONO) measurement uncertainty is estimated to be 25 %.

2.4 Stable species measurements

During the campaign, a wide variety of trace gases was measured (NO, NO_2, O_3, CO, HONO, PAN, HCHO, other aldehydes and ketones, and NMHC (C_4–C_{16}), listed in Table 1).

NO was measured by a commercial analyser model AC31M (Environnement S.A.) using ozone chemiluminescence. The NO analyser was weekly calibrated using a standard 200 ppb NO/Air mixture. Furthermore, multipoint calibrations (0–40 ppb), using the same gas cylinder and a dilution system, were carried out before and after the campaign. NO_2 was measured by a commercial analyser NO_xTO_y (Metair) using luminol chemiluminescence as described in details by Hasel et al. (2005). This analyser was calibrated twice, before and after the campaign, using a cylinder containing 200 ppb $NO_2^/$Air mixture and a dilution system.

Ozone was measured with an analyser model 49C (Thermo Environmental) using UV absorption. This instrument was calibrated before the campaign using a quantified ozone source (ANSYCO).

CO was measured by Gas Chromatography with Reduction Gas Detection. Detailed description of this technique is given in Gros et al. (1999).

PAN (PeroxyAcetyl Nitrate) was measured by Gas Chromatography with Electron Capture Detection (GC-ECD). The calibration of this instrument was performed, after the campaign, in a smog chamber (Wang et al., 2011) in which laboratory-synthesised PAN (Nielsen et al., 1982) was introduced and simultaneously measured by the GC-ECD and a FTIR (Fourier Transform Infrared spectrometer) instrument.

Nitrous acid (HONO) was measured by a wet chemical derivatization technique with sulphanilamide and N-ethylene diamine as derivating agent and a phosphate buffer at pH 7 as trapping solution. The detection of the azo-dye formed was made by a High Performance Liquid Chromatography (HPLC) with detection by visible absorption at 540 nm. The instrument for nitrous acid measurement has been described in detail by Afif et al. (2012). This instrument was calibrated before and after the campaign using nitrite liquid solutions at different concentrations.

The formaldehyde (HCHO) and other aldehydes and ketones, representing 20 oxygenated species, were trapped on DNPH cartridges with a 3h time resolution. The analysis of these cartridges was made by HPLC using the technique described by Detournay et al. (2011). The VOC measurements were made by two different techniques. A GC-FID, AirmoVOC from Chromatotec, was deployed to measure VOCs from C_3 to C_9. During the MEGAPOLI campaign this technique allowed measurements of 7 species from C_4 to C_6 including isoprene. This instrument was calibrated weekly using cylinders containing known mixtures of different VOCs. In addition, samples collected every three hours on Charcoal cartridges and analysed later by a GC-FID (Detournay et al., 2011) enabled measurement of 20 VOCs from C_7 to C_{16}. More details on VOC measurements can be found in Ait-Helal et al. (2012).

3 Model description

3.1 Simple quasi Photo Stationary State (PSS) approach

The SIRTA site is located in a semi-urban area, where NO_x concentrations reach up to some tenths of ppb. This site is thus dominated by intermediate or high NO_x conditions. Under high NO_x conditions the OH radical budget can be largely simplified by assuming that the loss of the sum of the radicals is governed by reaction of OH with NO and NO_2. To determine whether or not the radical chemistry in Palaiseau during MEGAPOLI is governed by high NO_x conditions, OH concentrations were estimated using simple Photo Stationary State (PSS) calculations constrained with measured data. The calculations were made with accounting for radical production from HONO, HCHO and O_3 photolysis and radical loss in reactions with NO and NO_2:

$$L_R = k_{OH+NO}[OH][NO] + k_{OH+NO_2}[OH][NO_2] \quad (R1)$$

$$P_{R1} = J(HONO)[HONO] + 2J(O^1D)[O_3]\Phi_{OH_1} + 2J(HCHO_{rad})[HCHO] \quad (R2)$$

P_R and L_R represent, respectively, the production and loss rates (in molecule $cm^{-3}\,s^{-1}$). The terms k_{OH+NO} and k_{OH+NO_2} represent the rate constants of the reactions between OH and NO and between OH and NO_2, respectively, and are temperature and pressure dependent (Atkinson et al., 2004). Φ_{OH_1} represents the fraction of O^1D formed by ozone photolysis which will react with H_2O to form OH. This rate is calculated using known rate constants for O^1D quenching reactions with N_2 and O_2 and known rate constants for reaction between O^1D and water (Dunlea and Ravishankara, 2004a, b). Since the $J(HCHO_{rad})$ was not measured, it has been estimated from the measured $J(NO_2)$ and $J(O^1D)$ data using the parameterization by Holland et al. (2003). In addition to these photolysis processes, a large source of OH in urban area can come from non-photolytic processes such as ozonolysis of alkenes (Kanaya et al., 2007) resulting in a radical production rate given by:

$$P_{R2} = P_{R1} + \sum k_{O_3+alkene}[alkene][O_3]\Phi_{OH_2} \quad (R3)$$

Φ_{OH_2} represents in this equation the radical (that is, OH, HO_2, RO, RO_2, RCO_3) yields from the respective reactions between ozone and alkenes and $k_{O_3+alkene}$ the rate constant of the reaction between O_3 and an alkene (Calvert et al., 2000).

The Photo Stationary State assumes that the radical production rate is balanced by the radical loss rate ($P_R = L_R$). Thus, the Photo Stationary State concentrations of OH derived from this equilibrium, considering the P_{R1} or P_{R2} production, are given by:

$$[OH]_{PSS1} = P_{R1}/(k_{OH+NO}[NO] + k_{OH+NO_2}[NO_2]) \quad (R4)$$

Table 1. Measurements and techniques during the MEGAPOLI summer campaign.

Species	Time resolution (min)/2σ uncertainties (%)/Detection limit	Instrumentation	Institution
OH	5/35/3.10^5 cm^{-3}	CIMS SAMU	LATMOS
ROx	5/45/10^6 cm^{-3}	CIMS SAMU	LATMOS
NO	1/5/0.5 ppb	Ozone chemiluminescence	LISA
NO_2	1/5/0.5 ppb	Luminol chemiluminescence	LISA
O_3	1/5/1 ppb	UV absorption	LISA
CO	15/10/1 ppb	GC-RGD	LSCE
PAN	15/10/10 ppt	GC-ECD	LISA
HONO	10/12/5–10 ppt	Wet chemical derivatization (SA/NED)/HPLC detection (NITROMAC)	LISA
HCHO, other oxygenated compounds	180/25/10 ppt	DNPH cartridges	EMD, LISA
VOC's (C_3–C_9)	30/15/50–100 ppt	GC-FID	LISA
VOC's (C_7–C_{16})	180/25/10 ppt	cartridges	EMD, LISA
Aerosol Surface Area	1/nc/nc	Aerosol Particle Sizer	PSI
Photolysis frequencies (J(NO2), J(O1D), J(HONO))	1–10/20–25/10^{-7}–5.10^{-5} s^{-1}	Filterradiometres, spectroradiometre (LI-1800)	LISA
RH, Temperature, Pressure, wind speed, wind direction	1/nc/nc	Wind sensor and multiplate radiation shield (Young)	LISA
Boundary Layer Height	60/nc/nc	Lidar	LMD

$$[\mathrm{OH}]_{\mathrm{PSS2}} = P_{\mathrm{R2}}/(k_{\mathrm{OH+NO}}[\mathrm{NO}] + k_{\mathrm{OH+NO_2}}[\mathrm{NO_2}]) \quad \text{(R5)}$$

These calculations were performed only for the days of the campaign when all parameters involved in the calculations were available. Despite this restriction, seven days of calculations could be made and compared to observations. The concentrations of alkenes of anthropogenic origin were under the detection limit of the GC-FID instrument, which is about 100 ppt, during the whole study period, except for methylpropene. The concentrations of 10 linear or branched alkenes (from propene to heptene) have been set to 100 ppt in the OH PSS_2 calculation in order to have a high limit estimation of the impact of alkenes on OH quasi-stationary levels. In addition to ozonolysis of these 10 alkenes, the ozonolysis of isoprene, α-pinene, β-pinene and limonene, all measured during MEGAPOLI, have been added to the OH source equation $(\mathrm{OH})_{\mathrm{PSS2}}$.

3.2 Box modelling with the Master Chemical Mechanism (MCM)

A comprehensive analysis of the radical chemistry during the MEGAPOLI summer campaign requires the use of a model where all the OH, HO_2 and RO_2 radical sources and sinks are taken into account. Radical concentrations and budgets were thus simulated with a box model constrained with all measured data using a detailed chemical scheme to represent organic chemistry. The MCM mechanism v3.1 (http://mcm.leeds.ac.uk/MCM) (Jenkin et al., 1997, 2007; Saunders et al., 2003; Bloss et al., 2005) was implemented in a zero dimensional photochemical box model. This mechanism was updated for the inorganic chemistry with kinetic data from SAPRC 07 (http://www.engr.ucr.edu/~carter/SAPRC/) (Carter, 2010). The MCM subset used in our model includes the oxidation of all measured organic species, containing around 5000 species and 14 000 reactions. Time integration was solved in the model using the two-step solver (Verwer et al., 1994, 1996).

Table 2. List of the 32 VOCs measured during MEGAPOLI summer campaign and constrained in the MCM model.

Compound Name		Time Resolution	Mixing Ratio (ppb)		
MCM	Name	(min)	Max	Averaged	Median
MEPROPENE	Isobutene	30	2.5	0.52	0.32
IC4H10	Isobutane	30	0.78	0.25	0.2
NC4H10	Butane	30	2.2	0.32	0.24
C5H8	Isoprene	30	2.7	0.34	0.25
IC5H12	Isopentane	30	2	0.28	0.17
NC5H12	Pentane	30	0.9	0.17	0.12
TOLUENE	Toluene	180	0.84	0.16	0.13
NC6H14	Hexane	30	0.27	0.1	0.09
EBENZ	Ethylbenzene	180	0.12	0.03	0.02
MXYL	M-Xylene	180	0.15	0.03	0.02
OXYL	O-Xylene	180	0.13	0.03	0.03
PXYL	P-Xylene	180	0.15	0.03	0.02
NC9H20	Nonane	180	0.07	0.01	0.01
APINENE	α-Pinene	180	0.23	0.04	0.03
BPINENE	β-Pinene	180	0.03	0.01	0.01
NC10H22	Decane	180	0.11	0.02	0.02
NC11H24	Undecane	180	0.07	0.02	0.01
NC12H26	Dodecane	180	0.12	0.02	0.01
CH3CHO	Acetaldéhyde	180	3.2	0.56	0.48
GLYOX	Glyoxal	180	0.41	0.03	0.02
ACR	Acrolein	180	0.09	0.01	0.01
C2H5CHO	Propanal	180	0.42	0.05	0.04
CH3COCH3	Acetone	180	6	1.2	1.1
MGLYOX	MethylGlyoxal	180	0.4	0.05	0.04
MACR	Methacrolein	180	0.41	0.05	0.03
MVK	Butenone	180	1.6	0.3	0.25
C3H7CHO	Butanal	180	0.05	0.01	0.01
MEK	Butanone	180	8.6	1.7	1.5
C3ME3CHO	3-Methylbutanal	180	0.15	0.02	0.01
C4H9CHO	Pentanal	180	0.08	0.01	0.01
C5H11CHO	Hexanal	180	0.57	0.04	0.02
BENZAL	Benzaldéhyde	180	0.31	0.02	0.02

The model was constrained with 10 min values of the following measured environmental parameters: relative humidity (RH), temperature, pressure, boundary layer height, $J(O^1D)$, $J(NO_2)$ and J(HONO). The non measured photolysis frequencies were calculated as a function of the solar zenith angle using the TUV radiation model and corrected with $J(O^1D)$ or $J(NO_2)$ measurements. The calculated photolysis frequencies were multiplied by the ratio between measured and TUV calculated $J(O^1D)$ for species photolyzed at wavelengths smaller than 330 nm and by the ratio between measured and TUV calculated $J(NO_2)$ for species photolyzed at wavelengths longer than 330 nm.

The model was also constrained for stable species with 10 min measurements of NO, NO_2, O_3, CO, CH_4, CO_2, HCHO, HONO, PAN, and 32 VOCs (listed in Table 2). In order to create this 10 min database, the species concentrations were averaged or linearly interpolated depending on their time resolution (see Table 1). No measurement of benzene and propane were available during the campaign. For the modelling calculations the concentrations of benzene and propane were estimated using their quadratic relationship with, respectively, toluene and butane. These relationships obtained during a previous preparation campaign conducted in June–July 2008 at the SIRTA provide a good correlation with R^2 of 0.71 and 0.83 for benzene/toluene and propane/butane, respectively. In order to test the influence of these two species on radical chemistry and an eventual error caused by the estimation of their concentrations, sensitivity tests were conducted by varying their concentrations by a factor of 10 covering the full range of atmospheric concentrations of these species in a semi-urban environment. The multiplication of benzene concentration by 10 or 0.1 led to minor differences in radical concentrations simulated by the model: respectively 0.05 % and 0.01 % for OH, 0.60 % and 0.06 % for HO_2 and 1.50 % and 0.10 % for RO_2. Similar minor differences were observed for propane, since multiplying

its concentration by 10 or 0.1 led, respectively, to modifications of 0.20 % and 0.02 % for OH, 0.60 % and 0.06 % for HO_2 and 0.20 % and 0.02 % for RO_2.

While most of the primary VOCs were measured, only some secondary VOCs were detected (HCHO, other aldehydes, some ketones...). These unmeasured secondary species could likely have an important influence on the RO_x formation, propagation and termination rates (Emmerson et al., 2005b; Volkamer et al., 2010; Kato et al., 2011; Liu et al., 2012). The concentrations of unmeasured secondary organic species were estimated following three distinct methods described below.

Method 1: formation of secondary species from the oxidation of the measured compounds up to a daily stationary state. Each day (from midnight to midnight) was simulated several times, constraining each time the model with the same measured data, until daily stationary concentrations were reached for the unmeasured secondary species. This daily steady state for unmeasured compounds was reached after 5 days. Each day of the campaign was considered independently and the unmeasured species concentrations were set to zero at the beginning of the next day to simulate. Such an approach has been used several times for similar studies (Carslaw et al., 2001; Emmerson et al., 2007; Kanaya et al., 2007; Elshorbany et al., 2009; Bloss et al., 2010). This version of the model is referenced as the 5-day spin up model hereafter and will be used as the reference model.

Method 2: accumulation of secondary species formed from the oxidation of measured compounds during a few hours at each data point. We have considered an accumulation time of 1 or 2 h. The unmeasured concentrations of secondary species were simulated for each 10 min data point for a prescribed time period (i.e. 1 or 2 h) with the constrained measured parameters held constant. As each 10 min dataset was considered independently, the concentrations of unmeasured species are then set to zero for the next time step of the simulation. These two model versions are referenced hereafter as the cumul1 h model and the cumul2 h model, respectively. The correlations between the radical concentrations determined with these two cumulative approaches and with the 5-day spin up model are presented in Fig. 1 (panel a to f). Compared to the reference model, the simulated OH concentrations are increased by 2.7 % for the cumul1h model while no modification are found for the cumul2h model; simulated HO_2 and RO_2 concentrations are reduced by 19 % and 30 % for the cumul1h model respectively and by 16 % and 23 % for the cumul2h model respectively. These results can be explained by the lower concentrations obtained for the unconstrained secondary VOCs with the 1 h and 2 h accumulation model versions.

Method 3: dilution of secondary species formed from the oxidation of measured compounds. The model was run over the full campaign, constrained with the 10 min measured data, with a dilution loss corresponding to a residence time of 1 or 2h for unmeasured secondary species. A 2-day spin up period was run at the beginning of the simulation to allow unconstrained VOCs to reach a stationary state. These versions of the model are called hereafter 1h dilution model and 2 h dilution model. The correlations between the radical concentrations obtained by these two approaches and the radical concentrations obtained with the reference model are shown in Fig. 1 (panel g to l). No significant differences are found between the radical concentrations estimated by the reference model and the ones estimated by the 2h dilution model (0.4, 0.9, 2.7 % for OH, HO_2 and RO_2 respectively). Higher differences are found for the 1h dilution model. Indeed, modelled OH concentrations are increased by 7.1 % and modelled HO_2 and RO_2 concentrations are reduced by 31 and 39 % respectively. These differences result from the lower concentrations simulated with the 1h dilution model for the non measured VOC.

None of these approaches is fully satisfactory to estimate the unmeasured VOCs concentrations (see Supplement S2). However, the various versions of the model are expected to encompass the concentration of non measured secondary VOC and therefore their influence on radical budget. Thus, two contrasted versions, the reference and the 1 h dilution, will be used for the comparison between measurement and model results.

Finally, dry deposition rates were assigned to stable species in the model and applied over the boundary layer for which the height was constrained in the model using in situ observations made at the measurement site (Haeffelin et al., 2011). The deposition velocities were taken from Derwent (1996) for NO_2 ($0.15\,cm\,s^{-1}$), HNO_3 ($2\,cm\,s^{-1}$), O_3 ($0.5\,cm\,s^{-1}$), SO_2 ($0.5\,cm\,s^{-1}$), PAN ($0.2\,cm\,s^{-1}$, assumed the same for all PANs species) and from Brasseur et al. (1998) for HCHO ($0.33\,cm\,s^{-1}$, assumed the same for all aldehydes), H_2O_2 ($1.1\,cm\,s^{-1}$), methyl- and ethyl- nitrate ($1.1\,cm\,s^{-1}$, assumed the same for all organic nitrates), and CH_3OOH ($0.55\,cm\,s^{-1}$ and assumed the same for all organic peroxides). For the multifunctional species, the highest deposition velocity by function was adopted. This means that if a species own several functions, the deposition velocity applied to this species is the one of the functions which has the highest deposition velocity. For the remaining MCM species, the dry deposition velocities have been set to a default value of $0.5\,cm\,s^{-1}$. A test was performed to evaluate the sensitivity to this default deposition velocity and simulations were conducted using values in the 0–$2\,cm\,s^{-1}$ range. The results show a low impact on the simulated radical concentrations. These results are reported in Table 3.

4 Results and discussion

4.1 Overview of measurement results

The measured concentration of inorganic species (NO_x, O_3 and HONO) and radical species (OH and (HO_2+RO_2))

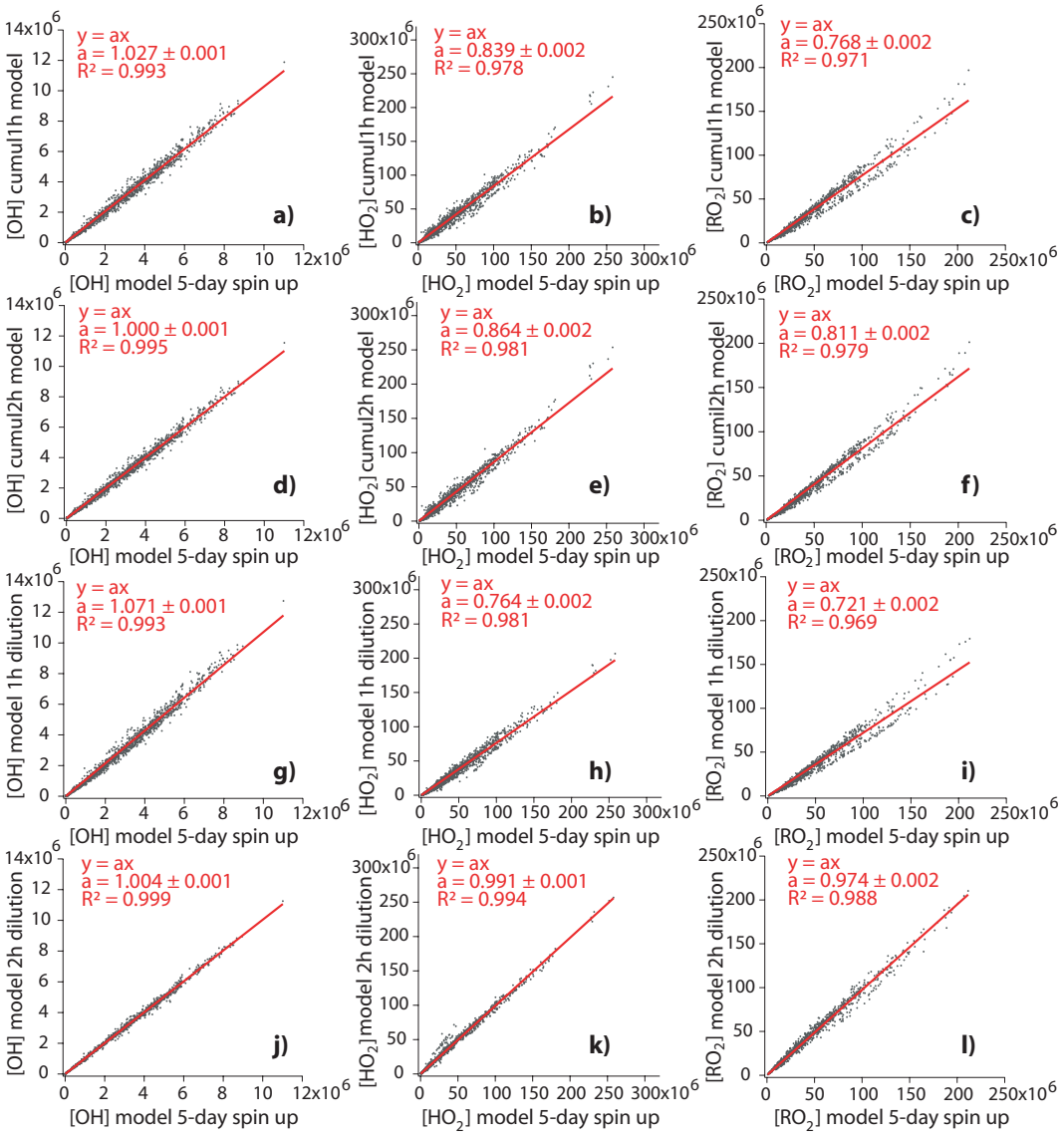

Fig. 1. Correlation between radical concentrations simulated by the three modelling procedures presented in Sect. 3.2. The panels **(a)** to **(c)** represent the correlations of radical concentrations (OH, HO_2 and RO_2) simulated by the cumul1h model and by the 5days spin up model. The panels **(d)** to **(f)**) represent the correlations of radical concentrations simulated by the cumul2h model and by the 5days spin up model. The panels **(g)** to **(i)** represent the correlations of radical concentrations simulated by the 1h dilution model and by the 5days spin up model. Finally, the panels **(j)** to **(l)** represent the correlations of radical concentrations simulated by the 2 h dilution model and the 5 days spin up model.

between the 9–26 July 2009 are shown in Fig. 2 together with the $J(O^1D)$ and wind direction. The mean diurnal profiles averaged every 10 min over the campaign period are shown in Fig. 3. During the campaign, cloudy weather conditions were prevailing with temperatures ranging between 283 K during the night and 305 K for the rare sunny days. The wind came mainly from westerly and south-westerly sectors bringing clean oceanic air masses. Some rare events with the wind coming from the east or south-east sectors resulted in more polluted air masses from more urbanised areas or, at least because of a longer residence time above continental land (Freutel et al., 2012) (e.g. on 21 July with concentrations of NO_2, O_3 and OH reaching on this day, 25 ppb, 70 ppb and 1.06×10^7 molecule cm^{-3} respectively).

During the whole studied period, OH concentrations exhibited a clear diurnal profile with daytime maxima of (3.5–10.1) $\times 10^6$ molecule cm^{-3} with mean maximum value of 4.2×10^6 molecule cm^{-3} at about 13:30 local time (LT). Diurnal variation of $J(O^1D)$ was similar to that of OH with an average daytime maximum around 14:00 LT of

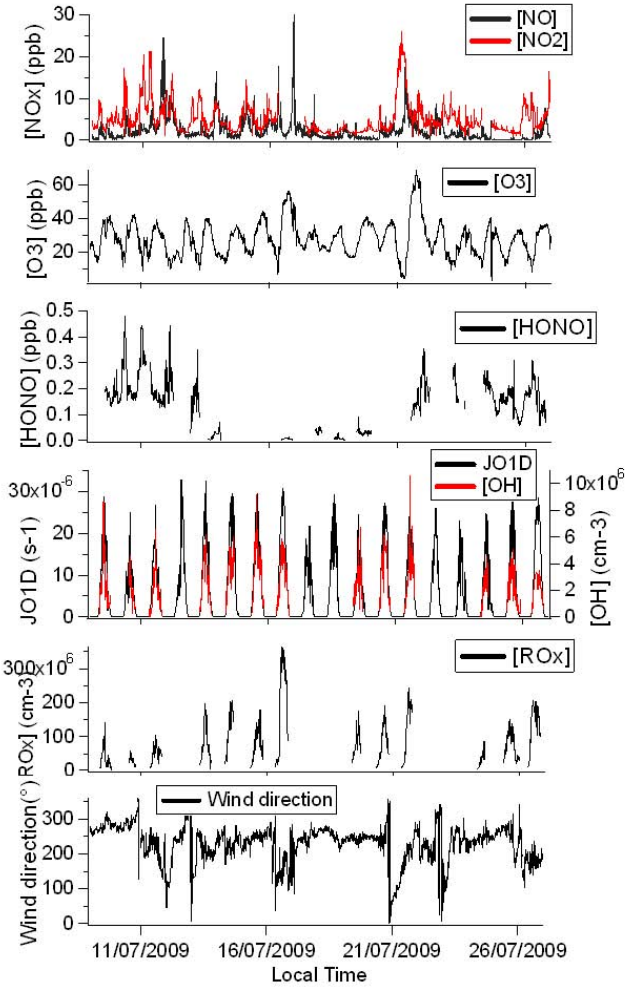

Fig. 2. 10 min data of NO_x, O_3, HONO, $J(O^1D)$, OH, RO_x and wind direction during the MEGAPOLI summer field campaign in Palaiseau, 9–26 July 2009.

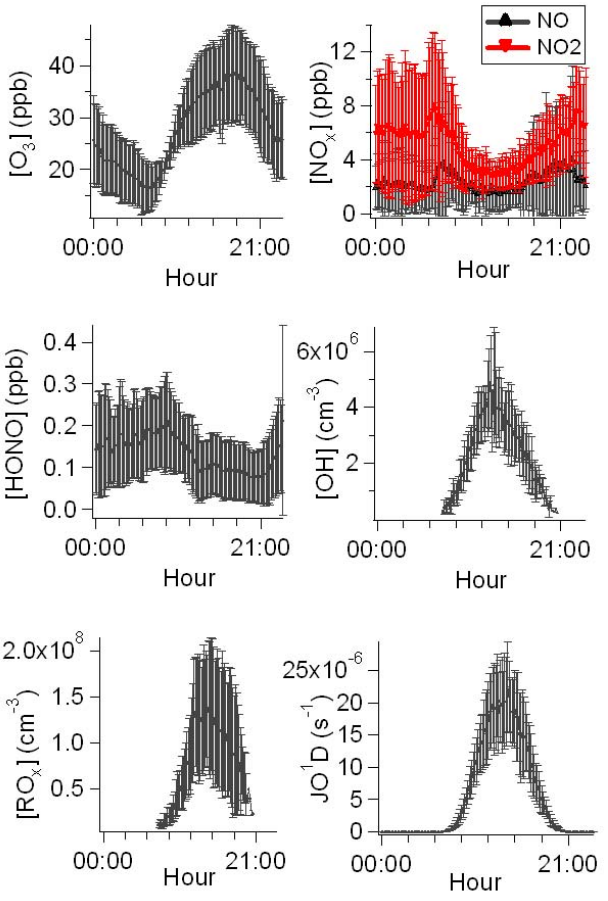

Fig. 3. Average diurnal 10 min profiles for O_3, NO_x, HONO, OH, $(HO_2 + RO_2)$ and $J(O^1D)$ during the MEGAPOLI summer campaign. Error bars correspond to standard deviation for the day to day variability.

about $2.2 \times 10^{-5}\,s^{-1}$. The correlation between OH and $J(O^1D)$ is discussed in Supplement S3. The (HO_2+RO_2) mean diurnal profile showed maximum value of about 1.4×10^8 molecule cm^{-3} around 14:00 LT.

O_3 showed a typical diurnal variation with averaged daytime maxima values of 38 ppb at about 17:00 LT. The mean daytime rush hour maxima for NO and NO_2 at around 07:00 LT were 4 ppb and 8 ppb, respectively. The HONO concentration levels were variable, up to 500 ppt, with the averaged daytime maximum of 210 ppt at around 09:00 LT. Furthermore, a detailed discussion of VOC results at SIRTA observatory can be found in Ait-Helal et al. (2012).

During MEGAPOLI summer campaign, the measurement site was thus characterised by intermediate NO_x levels (7 ppb in average for NO_x, 2.3 ppb and 5.1 ppb on average for NO and NO_2, respectively) and quite low O_3 levels (30 ppb in average). This is comparable with observations made in another suburban site in England, 40 km North-East of London in 2003 (Emmerson et al., 2007) with similar NO concentrations (2.9 ppb in average), but higher oxidant levels, i.e. NO_2 and O_3 (7.9 ppb and 46 ppb on average for NO_2 and O_3, respectively). This can be explained by the presence of a heatwave period during the UK TORCH campaign while cloudy weather conditions were prevailing during the MEGAPOLI summer campaign. The NO_x and O_3 levels encountered during the MEGAPOLI summer campaign are also very close to the ones observed during the PUMA campaign (Emmerson et al., 2005a), taking place 4 km south west from Birmingham city centre, when Atlantic air masses from the westerly sector reached the PUMA campaign measurement site (2.7 ppb, 6.6 ppb and 29 ppb on average for NO, NO_2 and O_3, respectively). However, for air masses coming from the easterly sector and passing over Birmingham city centre before arriving at the measurement site, higher NO_x and O_3 levels were observed (4.2 ppb, 14.4 ppb and 41.2 ppb in average for NO, NO_2 and O_3, respectively).

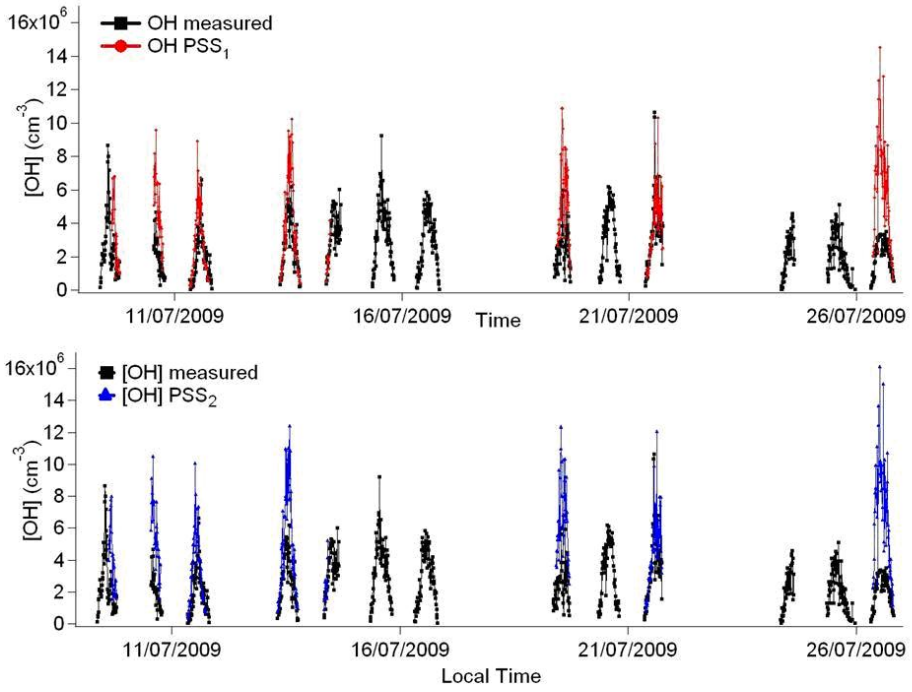

Fig. 4. Observed OH concentrations (black squares) compared with two PSS calculations including (PSS2) or not (PSS1) the ozonolysis of alkenes as OH source. The calculations of both PSS approaches are carried out only when all the parameters used in it are available.

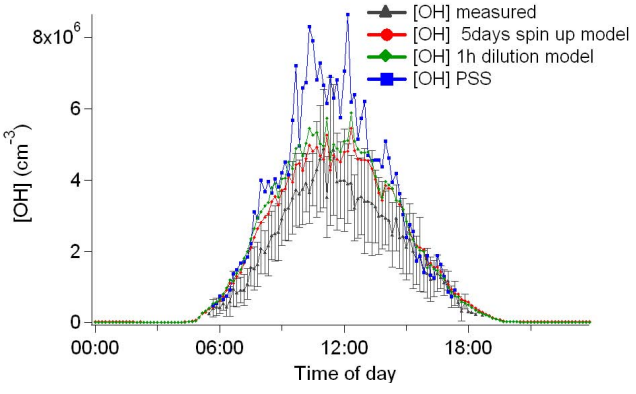

Fig. 5. Mean diurnal profiles of observed [OH] concentrations (black triangles), simulated [OH] concentrations with 5-day spin up approach (red circles) and with dilution of 1h lifetime approach (green diamonds) and [OH] calculated concentrations by PSS. The PSS results shown here are from Eq. (R4) (OH PSS1). Error bars correspond to standard deviation for day to day variability.

4.2 Comparison between PSS and measurement of OH concentrations

To assess if the radical chemistry in the suburban environment of Palaiseau can be explained by a simple Photo Stationary State approach, a comparison between PSS calculations and OH measurements has been made as presented in Fig. 4 (panel a and b respectively for $(OH)_{PSS1}$ and $[OH]_{PSS2}$) for the whole study period and in Fig. 5 for the average diurnal profiles. Correlations between observed and calculated OH concentrations from both PSS Eqs. (R4–R5) are shown in Fig. 6.

These comparisons show a large overestimation of OH by both PSS calculations. Figure 6 shows an overestimation of measurements of a factor of 1.50 for OH PSS_1 and 1.78 for OH PSS_2 on average. Including OH production via ozonolysis of alkenes leads to a rise of about 18 % of the OH concentrations calculated via PSS. This increase is a higher limit of the influence of alkenes on OH concentrations as the concentration of undetected alkenes has been set to the detection limit concentration of the instrument. Considering only measured alkenes in $[OH]_{PSS2}$ calculation, mainly methylpropene and isoprene, the increase of OH concentrations calculated via PSS_2 is only about 3 % compared with $[OH]_{PSS1}$.

Dependence of the ratio between calculated (via PSS_1) and observed OH concentrations is shown in Fig. 7 as a function of NO_x. The OH concentration tends to be in good agreement at high NO_x levels, with the ratio between calculation and observation near unity when NO_x is higher than 10 ppb. The PSS approach appears to be sufficient to explain OH concentrations in polluted environments, as it has been already shown in the highly polluted urban area of Santiago, Chile (Elshorbany et al., 2009), where similar OH concentrations are calculated (but not measured) by both the PSS approach and a box model containing the MCM and constrained with measurements. At lower NO_x, the OH

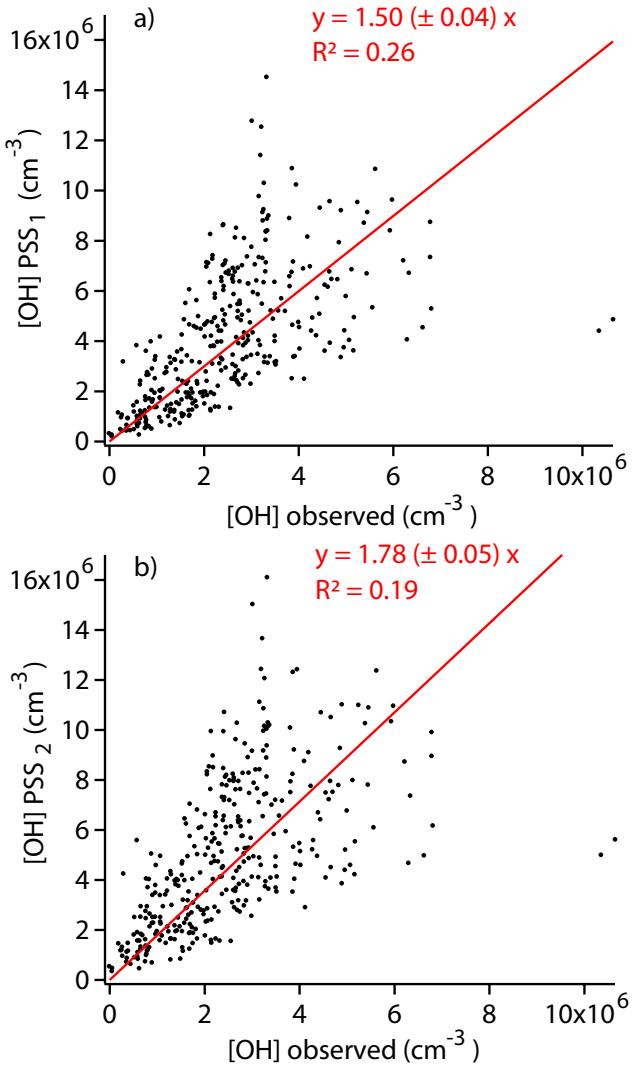

Fig. 6. Correlations between observed OH concentrations and OH PSS1 **(a)** and OH PSS2 **(b)** for the whole study period.

concentration is overpredicted by the calculation, the ratio between calculation and observation rising up to 5 at the lower NO_x. The simple PSS approach used here is inappropriate to explain the radical chemistry under intermediate or low NO_x conditions, such as in the suburban environment of Palaiseau. The lack of several loss pathways, such as peroxy radicals self termination reactions (HO_2+HO_2, or HO_2+RO_2) or reactions of peroxy radicals with NO_x, may explain this incapacity of PSS calculations to reproduce OH measurements. Thus, a more complex approach, taking into account an exhaustive chemical mechanism, is needed here to better represent the radical chemistry under our conditions.

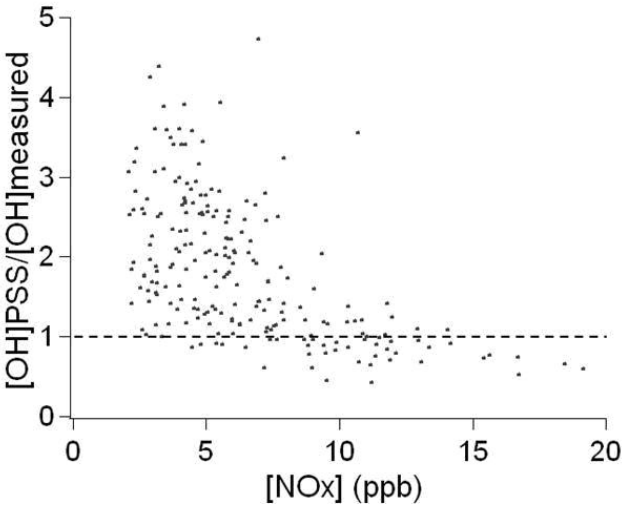

Fig. 7. Variation of the ratio between PSS calculated and observed OH concentrations with NO_x concentrations. The PSS calculated OH concentrations correspond to calculation from Eq. (R4) (OH PSS1). The dotted line represents a ratio between calculated and measured OH of 1.

4.3 Comparison between radical measurements and results from the box model

4.3.1 Model/measurements comparison of OH and (HO_2+RO_2) concentrations from model base run

The simulated OH time concentrations of the two extreme versions of the model, the reference model and the 1h dilution model, are compared to measurements in Fig. 8. The averaged diurnal profiles of OH observed, modelled and calculated with the PSS approach are shown in Fig. 5. The correlation between modelled and measured OH concentrations is presented in Fig. 9.

The model is in pretty good agreement with the observations for several days of the campaign (07/09; 07/11; 07/13; 07/15; 07/19; 07/20; 07/21), the difference being within the measurements uncertainties. Indeed, the differences between the simulated and measured OH concentrations on these days is lower than 15 % in average using the reference model and lower than 25 % in average using the 1h dilution model. On some other days, the model largely overestimates OH measurements (07/10; 07/14; 07/24; 07/25; 07/26). This overestimation is comprised, in average, between 38 and 67 % for the reference model and between 50 and 78 % for the 1h dilution model on these days. This overestimation between simulated and measured OH concentrations even reaches almost a factor of 2 on the 24th. The averaged diurnal profiles presented in Fig. 5 show that the model leads to a serious improvement of the estimation of the OH concentrations compared to the PSS calculations. Correlations between observed and simulated OH concentrations have been performed only when the measurements of the following constrained species were all

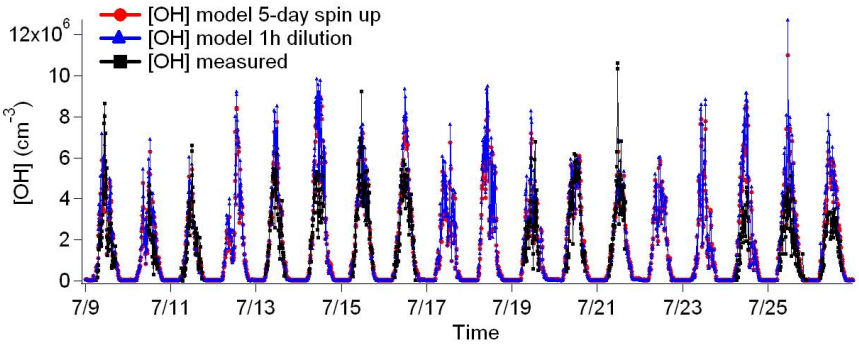

Fig. 8. Observed [OH] concentrations (black squares) compared with simulated [OH] concentrations by 5-day spin up scenario (red circles) and by 1h-dilution scenario (blue triangles) by MCM v3.1 implemented in a 0D boxmodel (see Sect. 3.2).

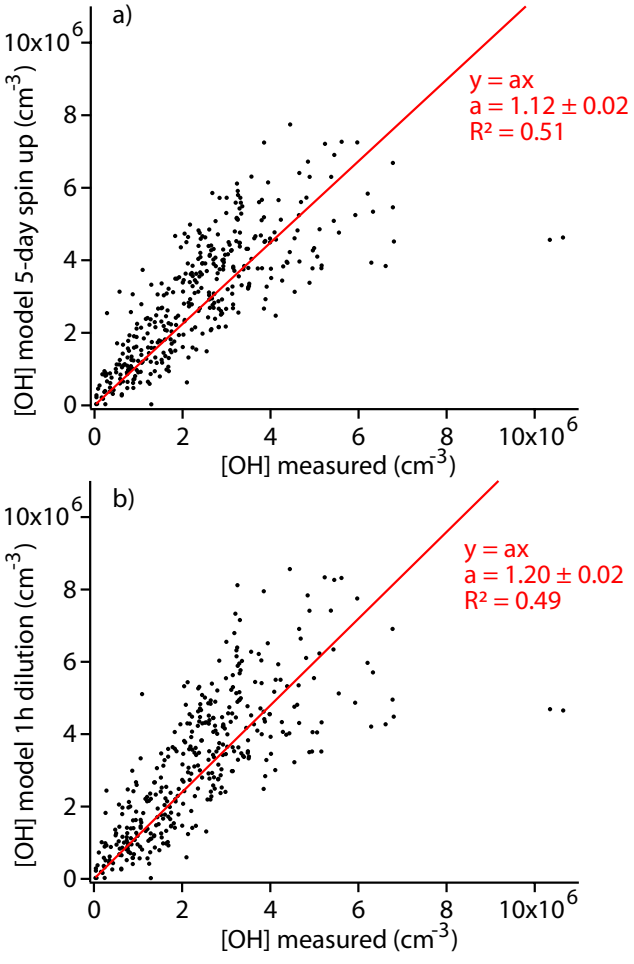

Fig. 9. Correlations between measured and modelled [OH] by two approaches for the whole study period. The red line represents linear regression forced by origin, with a slope of 1.12 and a correlation coefficient R^2 of 0.51 for the 5-day spin up model approach **(a)** and a slope of 1.20 and a correlation coefficient R^2 of 0.49 for the 1h dilution model approach **(b)**.

available: O_3, CO, NO, NO_2, HONO and HCHO. The linear regression slope between the modelled and observed OH concentrations are between 1.12 and 1.20 for various model versions whereas the one found for the correlation with PSS_1 calculations (Fig. 6) was 1.50. However, some discrepancies still remain and have to be investigated. Figure S4 in Supplement shows the evolution of the ratio between modelled (with the reference scenario) and observed OH concentrations with NO_x concentrations. No clear relationship can be found between NO_x levels and overestimation from the model, as it has been shown for the PSS calculations (Fig. 7). Thus, the model including a detailed description of radical sources and sinks enables to represent the processes involved in OH budget under intermediate and low NO_x levels better than the PSS calculations.

Simulated and measured peroxy radical ($HO_2 + \Sigma RO_2$) concentrations are compared in Fig. 10. Most of the time, the two extreme model versions allow to encompass the measured (HO_2+RO_2) concentrations (7/9; 7/10; 7/11; 7/13; 7/14; 7/15; 7/19; 7/21; 7/25; 7/26). However, both versions of the model largely overestimate measured (HO_2+RO_2) concentrations on 7/20 (by 76 % in average for the reference model and 33 % in average for the 1h dilution model) and 7/24 (by 150 % in average for the reference model and 96 % in average for the 1h dilution model) and underestimate the measurements on 7/16 (by 30 % in average for the reference model and 90 % in average for the 1h dilution model). The NO_x levels were quite low on 7/20 and 7/24 (NO_x concentrations being lower than 5 ppb during these two days) and quite high on 7/16 (NO concentrations reaching 18 ppb in the morning and 30 ppb in the evening). However, such NO_x levels were also encountered on some other days of the campaign without leading to similar trends in model discrepancies. Indeed, no clear relationship can be found between NO_x levels and model discrepancies (not shown). An analysis of retroplume calculations, performed using the FLEXPART model (Stohl et al., 2005), on these days shows no evidence of clear differences in air mass origins compared with other days. Indeed, similar retroplume origin is found

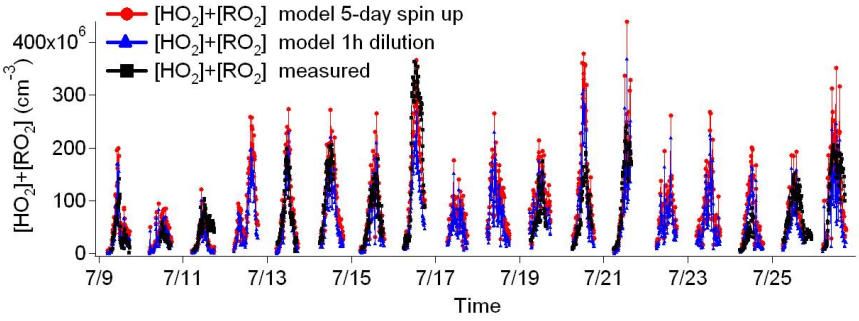

Fig. 10. Observed ($HO_2 + RO_2$) concentrations (black squares) compared to ($HO_2 + RO_2$) concentrations simulated by the 5-day spin up model approach (red circles) and by the 1h dilution model approach (blue triangles) by MCM v3.1 implemented in a 0D boxmodel (see Sect. 3.2).

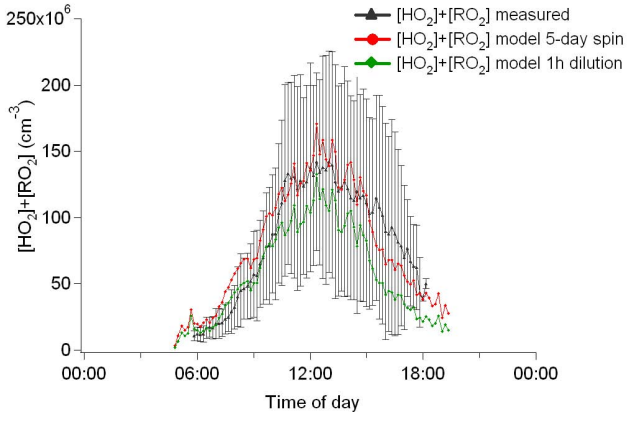

Fig. 11. Diurnal profiles of observed ($HO_2 + RO_2$) concentrations (black triangles) and simulated ($HO_2 + RO_2$) concentrations by the 5-day spin up model approach (red circles) and by the 1h dilution model approach (green diamonds). Error bars correspond to standard deviation for day-to-day variability of measured ($HO_2 + RO_2$).

for 07/16 and 07/21 and for 07/20, 07/24, 07/14 and 07/19, while no similar trends in model discrepancies are found for these days. The correlations between measured and simulated peroxy radical concentrations (see Fig.12) lead to good agreement on average with a slight overestimation of the reference model by a factor of 1.05 and an underestimation for the 1h dilution model with a slope of 0.76. As for OH correlation, these correlations apply only to the data where constraints for concentrations of O_3, CO, NO, NO_2, HONO and HCHO were not missing. The averaged diurnal profiles of measured and modelled (HO_2+RO_2) concentrations are shown in Fig. 11. The model using both scenarios allows reproducing the diurnal profile of measured (HO_2+RO_2) concentrations within the measurement uncertainties on average.

4.3.2 OH, HO_2 and RO_2 sensitivity to model constraints

Sensitivity tests have been performed to identify the parameters, measured or missing, that could have the largest impact on simulated radical concentrations. The model used to perform sensitivity tests is the 5-day spin up version of the model (reference model version). The changes induced by the various perturbations on OH, HO_2 and sum of organic peroxy radicals RO_2 concentrations are summarised in Table 3 and plotted in Fig. 13.

Most of the alkenes were present at a lower concentration than the detection limit of the instruments during the campaign. Even if present at low level, the impact of alkenes ozonolysis on radical formation can be important. Simulations have thus been conducted setting the concentrations of 12 branched or linear alkenes (from propene to hexene) to 100 ppt and 50 ppt respectively which corresponds to the upper estimation of the detection limit of the instrument and half of this detection limit. These simulations lead to a rise of radical concentrations in the model, with a larger impact of alkene ozonolysis on radical concentrations (OH, HO_2 and RO_2) during the night than during daytime, as expected. The increase of radical concentrations during daytime (06:00–17:30 UTC) compared with the base model simulation varied, for alkenes concentrations of 50 and 100 ppt, between 15 % and 26 % for OH, 48 % and 95 % for HO_2 and 44 % and 92 % for RO_2. These results highlight the large influence of alkene ozonolysis on RO_x concentrations and the importance of using a sensitive instrument to measure alkene species to study radical chemistry. However, this lack can explain neither the disagreement between the modelled and measured OH concentrations, nor the slight overestimation of simulated (HO_2+RO_2) concentrations, since the addition of alkenes tends to increase the overestimation of the model for all radicals.

NO_x measurement uncertainties can be high, especially at low levels (below a few ppb). Simulations have, thus, been performed varying constrained NO_x concentrations by 10 %. Simulated OH, HO_2 and RO_2 concentrations change by about +4.5/−4.6 %, +12.8/−11.7 % and +15/−13.8 % when constrained NO_x concentrations are decreased or raised by 10 % respectively.

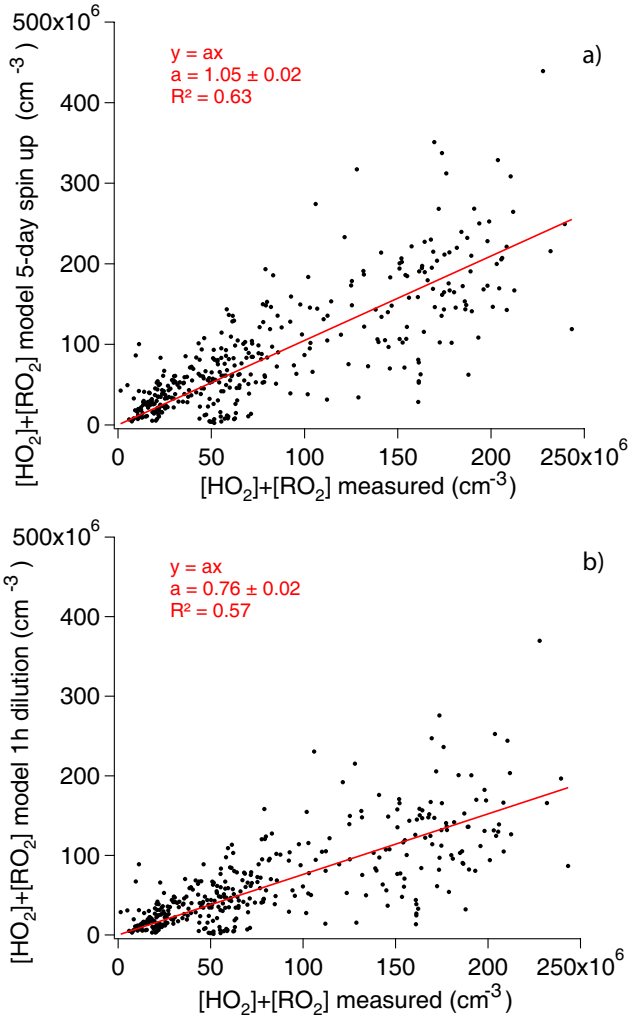

Fig. 12. Correlation between measured and modelled ($HO_2 + RO_2$) concentrations for the whole study period. The red line represents the linear regression forced through the origin, with a slope of 1.05 and a correlation coefficient R^2 of 0.63 for the 5-day spin up model approach **(a)** and with a slope of 0.76 and a correlation coefficient R^2 of 0.57 for the 1h dilution model approach **(b)**.

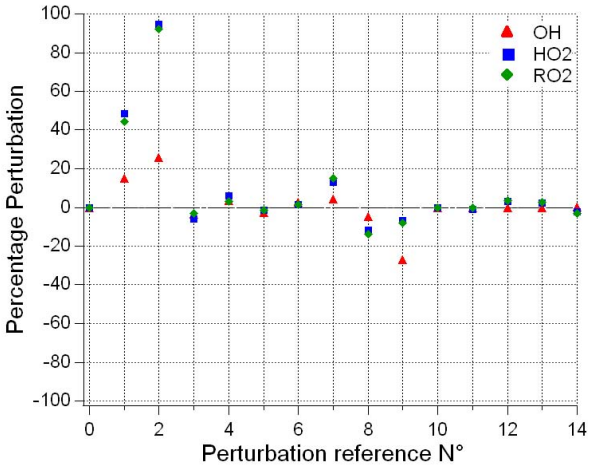

Fig. 13. Averaged percentage change in model OH (red triangles), HO_2 (blue squares) and organic peroxy radicals RO_2 (green diamonds) concentrations compared to the reference run for perturbations 1–14 (Table 3).

Quite high uncertainties are observed for species sampled by DNPH cartridges and then analysed by HPLC (25 %, see Table 1). Among them, the formaldehyde can represent an important source of radicals. Thus, simulations performed by varying constrained HCHO concentrations by 25 % have been performed. This leads to differences for modelled OH, HO_2 and RO_2 concentrations, respectively of −3.5/+3.3 %, −5.8/+5.8 % and −3.1/+3.2 % when HCHO concentrations are decreased or raised by 25 %.

Nitrous acid is one of the most important sources of OH in the atmosphere. The 2σ relative uncertainties in our HONO measurements are about 12 %, which is not negligible. Thus, simulations were performed varying constrained HONO concentrations by 10 %. This resulted in modifications of OH, HO_2 and RO_2 concentrations, respectively of −2.6/+2.5 %, −1.4/+1.5 %, −1.5 %/+1.6 % when HONO concentrations are decreased or raised by 10 %.

As an important number of photolysis frequencies are estimated in our model rather than being measured, uncertainties in their estimations cannot be excluded. To estimate the impact of such uncertainties on simulated radical concentration, simulations where $J(O^1D)$, $J(NO_2)$ and J(HONO) have been decreased by 20 % (which correspond to the estimated uncertainties in photolysis frequencies measurements) were performed. Other photolysis frequencies being estimated using the ratio between calculated and measured $J(O^1D)$ or $J(NO_2)$ (see Sect. 3.2), they have been decreased, too. Simulated OH concentrations decreased by 27 % whereas HO_2 and RO_2 are less affected, their predicted concentrations being decreased by 6.8 % and 8.2 %. Thus, these uncertainties in photolysis frequencies could be one of the reasons for the 5-day spin up model overestimation compared with the radical measurements.

Simulations have been run adding an uptake of HO_2 and CH_3O_2 on aerosol surface to the 5-day spin up model. The results of the model with the new scenarios compared with the measurements are shown in Fig. S5 in Supplement, as well as a discussion of these results. The changes observed in simulated radical concentrations are also listed in Table 3 and shown in Fig. 13. These changes were very low (0.1–0.4 % for OH, 0.2–1.1 % for HO_2 and 0.1–0.4 % for RO_2). Under the conditions encountered during the MEGAPOLI summer campaign, the addition of HO_2 and CH_3O_2 uptake on the aerosol surface by far cannot resolve the overestimation of simulated OH and (HO_2+RO_2) concentrations, since the aerosol surface area was probably too small.

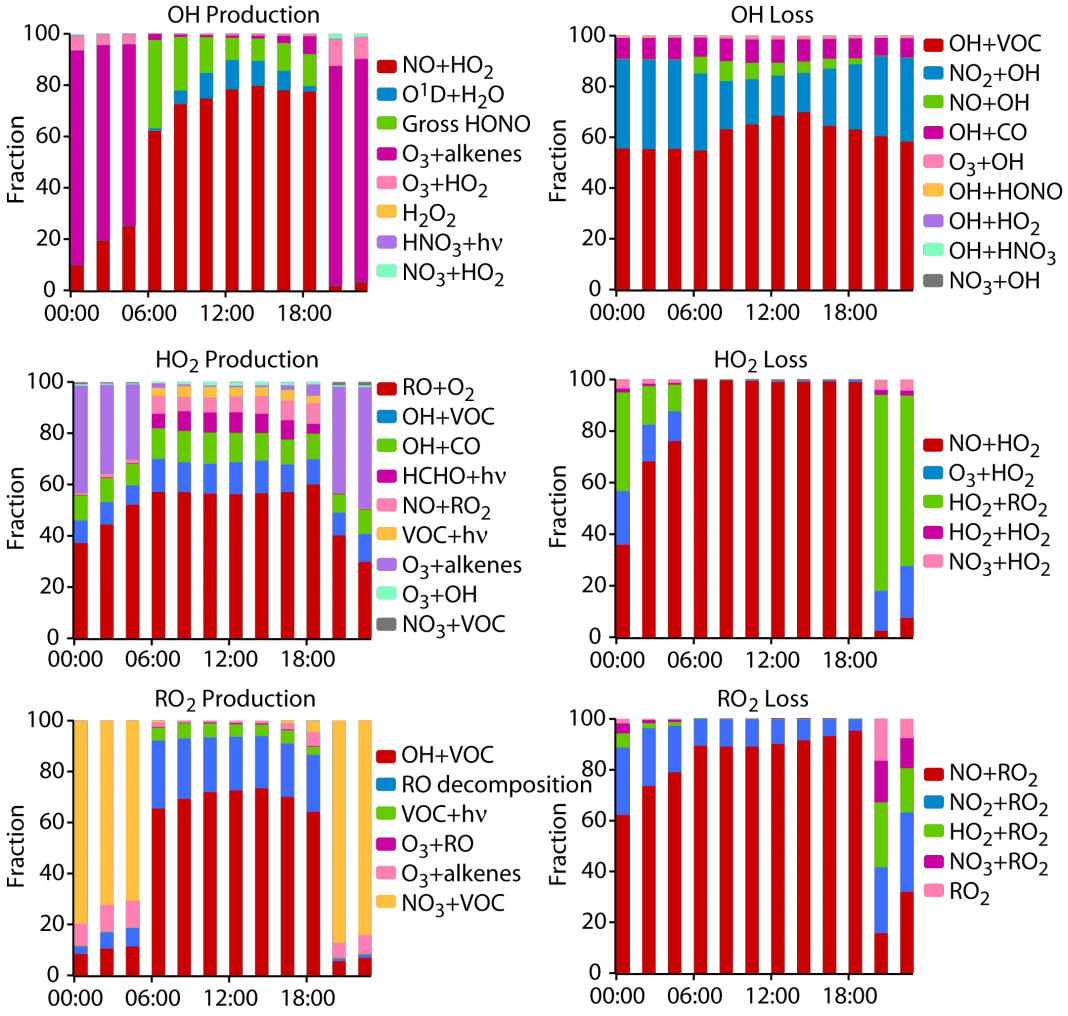

Fig. 14. Fraction of different processes involved in the production and loss of OH, HO_2 and RO_2 for a one day simulation (5-day spin up model) constrained with mean diurnal campaign measurements of all species and parameters.

The addition of alkenes and the reduction of NO_x concentrations lead to a significant rise of simulated OH, HO_2 and RO_2 concentrations. The decrease of photolysis frequencies and the rise of NO_x concentrations reduce significantly the simulated radical concentrations. On the contrary, the variations of HONO and HCHO concentrations, in the range of measurement uncertainties, lead to small changes in simulated radical concentrations. To summarize, these sensitivity tests have highlighted that uncertainties in simulated radical concentrations may partly come from measurement uncertainties of some species and parameters involved in radical initiation or termination processes and from the lack of anthropogenic alkene measurements.

4.4 Radical budget analysis

A radical budget analysis was carried out to investigate the key processes driving the radical initiation, propagation and termination during the MEGAPOLI summer campaign at the SIRTA observatory. The results presented here are from a one-day simulation performed with the reference model version. To constrain the model, averaged observed diurnal campaign concentrations have been used.

Figure 14 represents the fraction of the different processes involved in the production and loss of OH, HO_2 and RO_2. The OH production is mainly dominated by the NO + HO_2 reaction during the day (60–80 %), while reactions between O_3+alkenes and O_3 +HO_2 dominate during the night (70–80 % for the reaction O_3 + alkenes and 5–10 % for the reaction O_3+ HO_2). During the early morning, the second most important OH source just after the reaction between NO + HO_2 is HONO photolysis (contributing to more than 30 % to OH production). The contribution of HONO photolysis then decreases to reach a minimum of approximately 10 % between 12:00 and 14:00 UTC. This decrease is due to the diminishing of HONO concentrations observed in daytime hours because of its fast photolysis. The noontime OH

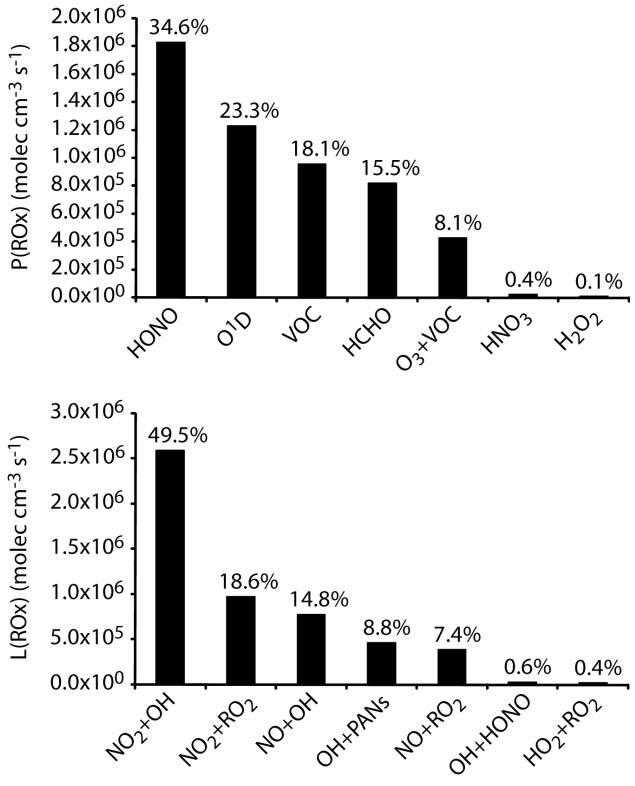

Fig. 15. Model calculated radicals initiation and termination rates averaged between 06:00 and 18:00 UTC for a one day simulation (5-day spin up model) constrained with mean daily campaign measurements of all species and parameters.

production through HONO photolysis stays significant and almost equivalent to the OH production through the reaction between O^1D and water. Quite high HONO concentration of approximately hundred ppt remains throughout the day. The contribution of the reaction between O^1D and water to OH production rises during morning hours and reaches its maximum (around 10 %) at 12:00 UTC with the maximum of photolysis. Other processes are negligible for OH production throughout the day.

OH sinks are dominated by reactions of OH with VOCs which contribute at a fraction higher than 55 % all along the day and reach almost 65 % during noontime hours. These reactions act as propagation reactions, leading mainly to RO_2 formation (∼81 % in average) but also directly to HO_2 formation at a non negligible fraction (∼15 % in average). The VOCs removing predominantly OH are isoprene, methyl-propene, formaldehyde, methyl-vinyl-ketone, acetaldehyde and methyl-ethyl-ketone in this order of importance. The fraction of measured VOC responsible for the OH loss compared to the fraction of unmeasured species was quantified. Indeed, this fraction is comprised between 70 and 80 % during daytime. This result is similar to that of Kato et al. (2011) who found that the contribution of the unidentified VOCs to OH reactivity was about 22 % of the total VOC for a suburban site located about 30 km from Tokyo city centre. The other main OH loss process is the reaction between OH and NO_2 which leads to the formation of HNO_3. This reaction is a radical termination, as the recycling of OH by HNO_3 photolysis is very slow and HNO_3 deposition is its main sink. The reaction between OH and NO_2 represents more than 30 % of OH loss during the night and almost 20 % during the day. During sunlight hours, the reaction between OH and NO represents approximately 5 % of OH loss processes. However, this reaction cannot be considered as a real radical sink since it leads to HONO formation which recycles OH by photolysis. The reactions between OH and CO lead to HO_2 formation and thus to radical propagation and represents almost 10 % of OH loss processes throughout the day. Other processes leading to OH loss are negligible all day long.

The production of HO_2 is mainly dominated by the reaction of propagation between RO and O_2 with a contribution to total HO_2 production representing of more than 40 % all day long and reaching 50 % during daytime. The contribution to total HO_2 production of other reactions of propagation through the OH to HO_2 pathway represents approximately 20 % all along the day. These propagation reactions are the reaction of OH with CO, O_3 and different VOCs. Another propagation pathway is the reaction between RO_2 and NO which represents 6–7 % of the total HO_2 production during daytime hours (between 06:00 and 18:00 UTC) but is almost inexistent during night time. During daytime, HO_2 initiation is nearly entirely due to the photolysis of HCHO and VOCs (other aldehydes and ketones). The contribution to total HO_2 production from these reactions is 10–20 % with maximum around noon. The HCHO photolysis accounts for almost twice the other aldehydes and ketones photolysis in terms of HO_2 production.

During the day, the HO_2 loss is almost exclusively due to its reaction with NO which leads to the formation of OH and NO_2. During the night, NO concentrations decrease and self radical reactions become fast enough to compete with the reaction between HO_2 and NO and to play a role in HO_2 loss. Indeed, during the late evening, the reaction between HO_2 and RO_2 reaches a contribution of almost 80 % of the HO_2 loss while the contribution of self reaction of HO_2 remains very low.

During the day, the main RO_2 production is due to the reaction of VOCs with OH. These reactions account for 60 to 70 % of RO_2 production with a maximum of the contribution reached at the maximum of photolysis. The second main daily RO_2 production is due to the RO decomposition which contributes up to 20 % all along the daytime hours. Thus, during sunlight hours RO_2 production is dominated by propagation reactions to around 80–90 %. The remaining RO_2 production during the day is due to initiation reactions mainly dominated by VOC (aldehydes and ketones) photolysis between 3 and 5 % of total RO_2 production. During the night the RO_2 production is dominated by the reaction of the NO_3

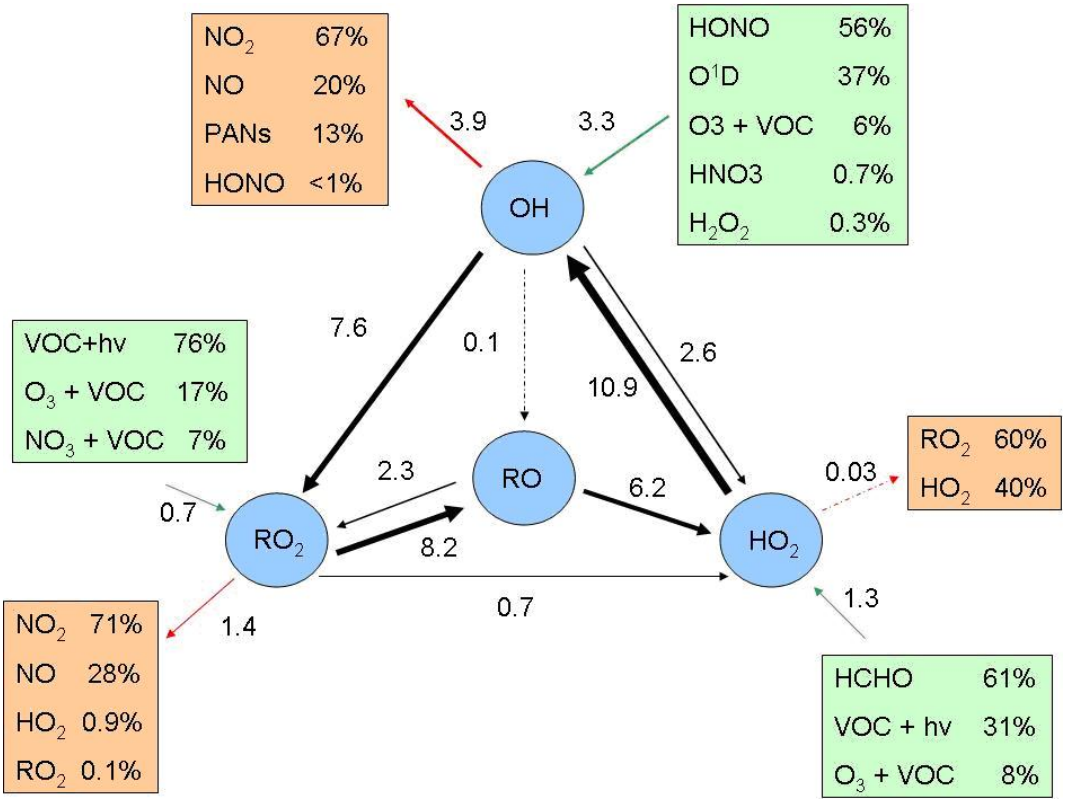

Fig. 16. Rate of radical initiation (green arrows), propagation (black arrows) and termination (red arrows) averaged between 06:00 and 18:00 UTC. These calculations are from a one day simulation (5-day spin up model) constrained with mean diurnal campaign measurements of all species and parameters. The numbers represent the rates in 10^6 molecule cm^{-3} s^{-1}.

radical with VOCs accounting for 70–90 % of the RO_2 production.

The RO_2 loss is dominated by the reactions between RO_2 and NO. These reactions account for 90 to 95 % of total RO_2 loss during the day and lead to the formation of RO, corresponding to propagation reactions, or of organic nitrates, corresponding to a radical sink. During the day the remaining RO_2 loss (approximately 5–10 %) is due to the reaction between RO_2 and NO_2. These reactions lead mainly to the formation of PANs. During the night, as for HO_2, radical self reactions become fast enough to compete with other reactions and play a role in RO_2 loss.

Figure 15 presents the radical initiation and termination rates for different reactions, averaged over daytime hours (06:00–18:00 UTC), as well as their contribution in the total radical initiation and termination. In other words, it presents sources and sinks for the $RO_x = OH + HO_2 + RO + RO_2$ budget. As it has been observed in many recent studies in both urban or rural environments (Ren et al., 2003b; Kleffmann et al., 2005; Ren et al. 2006; Dusanter et al., 2009; Elshorbany et al., 2009), HONO photolysis is a major radical source all over the day and not just during morning hours. Considering gross HONO photolysis, it accounts for approximately 35 % of total radical initiation, which is comparable to what Dusanter et al. (2009) found in Mexico City (34.5 %). However, subtracting the reaction between OH and NO to consider the net HONO source, its contribution to radical initiation falls to 23 % which still represents an important radical initiation pathway all over the day. The other reactions contributing to radical initiation are the reaction between $O(^1D)$ and water (23.3 %), photolysis of aldehydes (other than HCHO) and ketones (18.1 %), HCHO photolysis (15.5 %) and alkenes ozonolysis (8.1 %). However, it is important to note that the radical initiation via aldehydes (other than HCHO) and ketones photolysis is only due to approximately 30 to 50 % of measured species, the remaining fraction being unmeasured species especially dicarbonyls which were formed in the model. Thus, an important error can be made in the estimation of this radical initiation pathway. Moreover, simulations performed with the 1 h dilution model version (see Sect. 3.2), show results different from the 5-day spin up model version concerning radical initiation. Indeed, the radical initiation via aldehyde (other than HCHO) and ketones photolysis is less important and represents only 9.5 % of total radical initiation on a daily basis, behind HONO photolysis (40 %), reaction between $O(^1D)$ and water (27 %) and HCHO photolysis (17 %). The radical termination appears to be largely dominated by the reaction between OH and NO_x,

Table 3. OH, HO_2 and sum of organic peroxy radicals RO_2 sensitivities to model constraints and parameters. Sensitivity tests have been conducted over the full campaign period.

Number	Perturbation	Percentage Perturbation in		
		OH	HO_2	RO_2
0	Reference run	0	0	0
1	addition of alkenes at 50 ppt	14.9	48.3	44.4
2	addition of alkenes at 100 ppt	25.9	94.5	92.1
3	HCHO −25 %	−3.5	−5.8	−3.1
4	HCHO +25 %	3.3	5.8	3.2
5	HONO −10 %	−2.6	−1.4	−1.5
6	HONO +10 %	2.5	1.5	1.6
7	NO_x −10 %	4.5	12.8	15
8	NO_x +10 %	−4.6	−11.7	−13.8
9	$J \times 0.8$	−27	−6.8	−8.2
10	addition of HO_x uptake on aerosols with $\gamma_{HO_2} = 0.2$	−0.1	−0.2	−0.1
11	addition of HO_x uptake on aerosols with $\gamma_{HO_2} = 1$	−0.4	−1.1	−0.4
12	deposition of other species than those listed in Sect. 3.2 set to 0 cm s^{-1}	−0.2	3.1	3.6
13	deposition of other species than those listed in Sect. 3.2 set to 0.1 cm s^{-1}	−0.1	2.1	2.5
14	deposition of other species than those listed in Sect. 3.2 set to 2 cm s^{-1}	0.3	−2.4	−2.9

the reaction between RO_2 and NO_x and the reaction between OH and some PANs. It also appears that, during the day, the self reactions between radicals (HO_2+HO_2, HO_2+RO_2 and RO_2+RO_2) are negligible because of the quite high NO_x level at Palaiseau during the MEGAPOLI summer campaign. The importance of termination reactions between RO_2 and NO or NO_2, not taken into account in PSS calculations, can explain the incapacity of PSS calculations to reproduce OH concentrations while better results are observed for model calculations, where these reactions are included.

Daily averages (06:00–18:00 UTC) of initiation, propagation and termination rates are shown in Fig. 16. Averaged initiation and termination rates over the daytime hours are in balance around 5.3×10^6 molecule cm^{-3} s^{-1}. These rates are approximately five times lower than the initiation and termination rates observed during MCMA-2006 by Dusanter et al. (2009) in the centre of Mexico City. These observed differences are mainly due to far less polluted conditions, characterised by lower NO_x and VOCs levels, and less intense sunlight at SIRTA. However, we encountered closer total initiation and termination rates as Kanaya et al. (2012) in Jülich, Germany, in July 2005, where the total initiation rate in the period 12:00–15:00 UTC was comprised around 1.5×10^7molecule cm^{-3} s^{-1}, while we found approximately 1.0×10^7molecule cm^{-3} s^{-1} total initiation rate in the period 12:00–16:00 UTC. This corresponds to rather unpolluted conditions at the SIRTA site under the campaign conditions when most often oceanic air masses with little urban pollution were sampled.

5 Conclusions

The MEGAPOLI summer campaign provides an opportunity to assess our current knowledge of atmospheric gas chemistry and to provide a description of radical cycling reactions in a suburban environment. This was possible thanks to the large number of gaseous species and environmental parameters measured during this experiment concurrently with OH and (HO_2+RO_2) measurements. OH and (HO_2+RO_2) were measured during the campaign and showed typical diurnal profiles with daytime maxima around solar noon of $(3.5–10.6) \times 10^6$ and $(1.1–3.6) \times 10^8$ molecule cm^{-3}, respectively.

OH Photo Stationary State (PSS) calculations were performed and compared with OH measurements. This comparison shows a systematic overestimation of the calculation especially at low NO_x levels (<5 ppb). Then, a photochemical zero-dimensional box model, incorporating the Master Chemical Mechanism (MCM), was constrained by all measured parameters. This model was used to calculate radical concentrations (OH and (HO_2+RO_2)) as well as their rates of initiation, propagation and termination. One of the challenges encountered with such a method was to estimate the unconstrained secondary organic compounds. To do so, several versions of the model were tested and compared with

a reference model version. While the different approaches led to slight modifications of estimated OH concentrations (0.4 to 6.0 %), more important changes were observed for estimated HO_2 and RO_2 concentrations (16 to 31 % for HO_2 and 23 to 39 % for RO_2) excepted for the 2 h dilution model version where no significant differences were observed compared with the base case scenario (0.4, 0.9 and 2.7 % for OH, HO_2 and RO_2 respectively).

Based on the reference model simulations, the modelled OH and (HO_2+RO_2) concentrations were overestimated on average by factors of 1.12 and 1.05, respectively, which is pretty satisfactory given measurement uncertainties, and similar to some previous studies in suburban or remote environment. Based on the 1 h dilution simulations, OH concentrations were still overestimated (factor of 1.2) while (HO_2+RO_2) concentrations were in average underestimated by a factor of 0.76. The approach used in the 1h dilution model scenario led to lower formation of secondary VOCs and therefore to lower OH reactivity, but also to a decrease of radicals sources through OVOC (Oxygenated VOC) photolysis, compared with the reference scenario. This lower amount of secondary VOCs leads to underestimation of (HO_2+RO_2) concentrations while the overestimation of OH concentrations became slightly worse. These results point out the difficulty and the importance of the way this unmeasured secondary material is estimated by the model. Therefore, we advise to perform measurements of secondary VOCs as exhaustive as possible, especially for multifunctional ones in future campaigns. However, the use of the different versions of the model presented in this study allows encompassing the concentration of non measured VOCs and therefore their influence on radical budget.

The fact that modelled radical concentrations calculated with the reference model version were slightly overestimated indicates that some processes might be missing or might not be well estimated in the model. Therefore, the impact of the addition of HO_x uptake on aerosol surfaces in the model has been investigated, showing changes in modelled radical concentrations not important enough to explain the discrepancies between the model and the measurements. Other sensitivity tests had shown high model sensitivity to photolysis rates, NO_x and alkenes. Moreover, the sensitivity tests conducted in this study highlight the fact that uncertainties in model results could come from uncertainties in the measurement of some constrained parameters and species, or from the lack of anthropogenic alkenes measurements.

The analysis of the radical budget indicated that radical initiation resulted from several photolytic processes during the MEGAPOLI summer campaign. During daytime hours (06:00–18:00 UTC), the model predicted that the photolysis of HONO (34.6 %), the reaction between $O(^1D)$ and water (23.3 %), the photolysis of aldehydes (other than HCHO) and ketones (18.1 %) and the photolysis of HCHO (15.5 %) were the main sources of RO_x. However, the high contribution of the photolysis of aldehydes (other than HCHO) and ketones found by the model needs to be balanced by the fact that a high proportion of estimated secondary VOCs were involved in this radical production pathway (more than 50 %). Furthermore, the importance of the secondary VOC photolysis pathway was lowered when other model versions for the unconstrained species calculation were used. Production of OH from alkenes ozonolysis was found to be of minor importance (8.1 %) considering the absence of linear and branched alkenes of anthropogenic origin in model constraints because of their very low concentration levels during the MEGAPOLI summer campaign.

The analysis of the radical budget highlights also the importance of reactions between RO_2 and NO_x as radical termination reactions (approximately 26 % of total radical loss processes). These reactions were not taken into account in PSS calculations. This can explain the better agreement between the modelled and measured radical concentrations compared to the agreement between OH concentrations measured and estimated with PSS calculations. The total initiation and termination rates were in balance, around 5.3×10^6 molecule cm^{-3} s^{-1}, and similar to other ones found during previous studies in suburban or remote areas but far lower than other ones found in previous urban field campaigns.

Supplementary material related to this article is available online at: http://www.atmos-chem-phys.net/12/11951/2012/acp-12-11951-2012-supplement.pdf.

Acknowledgements. The research leading to these results has received funding from the European Union's Seventh Framework Programme FP/2007-2011 under grant agreement no. 212520.

The authors also acknowledge the ANR through the MEGAPOLI PARIS and INSU/ LEFE through the MEGAPOLI France project for their financial support. Moreover, the research leading to these results has been carried out in the framework of a thesis supported by CNRS grant.

The authors also want to thank Eurochamp-2 (EU-FP7 grant agreement no. 228335) for supporting intercalibration exercises, Birger Bohn, Forschungszentrum Jülich, Germany, for the calibration of the $J(NO_2)$ filter radiometer and the SAOZ network for their O_3 column data. Moreover, the authors acknowledge the team from the SIRTA observatory for their technical support. Acknowledgments are extended to J-C. Dupont for providing the boundary layer height retrievals used in this study and to R. Sarda and J. Nicolas for CO measurements. A. Stohl and S. Eckhardt are also thankfully acknowledged for providing the retroplume calculations.

Edited by: P. Monks

The publication of this article is financed by CNRS-INSU.

References

Acker, K., Moller, D., Wieprecht, W., Meixner, F. X., Bohn, B., Gilge, S., Plass-Dulmer, C., and Berresheim, H.: Strong daytime production of OH from HNO2 at a rural mountain site, Geophys. Res. Lett., 33, L02809, doi:10.1029/2005GL024643, 2006.

Afif, C., Jambert, C., Colomb, A., Eyglunent, G., Borbon, A., Daële, V., Doussin, J. F., and Perros, P. E.: NitroMAC: an instrument for the measurement of HONO, Intercomparison with LOPAP, Water Air. Soil. Poll., submitted, 2012

Ait-Helal, W., Borbon A., Sauvage S., De Gouw, J. A., Colomb A., Beekmann, M., Afif C., Durand-Jolibois, R., Fronval, I., Grand, N., Leonardis T., Michoud V., Miet K., Perrier, S., Siour G., Zapf, P., Doussin J. F., Lopez M., Gros V., Freutel F., Schneider J., Crippa M., Prevot A. S. H., and Baltensperger U., N. Locoge : I/VOC in sub-urban Paris: variability, origin and importance in SOA formation, Atmos. Chem. Phys. Discuss., in preparation, 2012.

Atkinson, R., Baulch, D. L., Cox, R. A., Crowley, J. N., Hampson, R. F., Hynes, R. G., Jenkin, M. E., Rossi, M. J., and Troe, J.: Evaluated kinetic and photochemical data for atmospheric chemistry: Volume I – gas phase reactions of O_x, HO_x, NO_x and SO_x species, Atmos. Chem. Phys., 4, 1461–1738, doi:10.5194/acp-4-1461-2004, 2004.

Aumont, B., Chervier, F., and Laval, S.: Contribution of HONO sources to the $NO_x/HO_x/O_3$ chemistry in the polluted boundary layer, Atmos. Environ., 37, 487–498, 2003.

Berresheim, H., Elste, T., Plass-Dulmer, C., Eisele, F. L., and Tanner, D. J.: Chemical ionization mass spectrometer for long-term measurements of atmospheric OH and H_2SO_4, Int. J. Mass. Spectrom, 202, 91–109, 2000.

Bey, I., Aumont, B., and Toupance, G.: A modeling study of the nighttime radical chemistry in the lower continental troposphere 2. Origin and evolution of HO_x, J. Geophys. Res., 106, 9991–10001, 2001.

Bloss, C., Wagner, V., Jenkin, M. E., Volkamer, R., Bloss, W. J., Lee, J. D., Heard, D. E., Wirtz, K., Martin-Reviejo, M., Rea, G., Wenger, J. C., and Pilling, M. J.: Development of a detailed chemical mechanism (MCMv3.1) for the atmospheric oxidation of aromatic hydrocarbons, Atmos. Chem. Phys., 5, 641–664, doi:10.5194/acp-5-641-2005, 2005.

Bloss, W. J., Camredon, M., Lee, J. D., Heard, D. E., Plane, J. M. C., Saiz-Lopez, A., Bauguitte, S. J.-B., Salmon, R. A., and Jones, A. E.: Coupling of HO_x, NO_x and halogen chemistry in the antarctic boundary layer, Atmos. Chem. Phys., 10, 10187–10209, doi:10.5194/acp-10-10187-2010, 2010.

Brasseur, G. P., Hauglustaine, D. A., Walters, S., Rasch, P. J., Muller, J. F., Granier, C., and Tie, X. X.: MOZART, a global chemical transport model for ozone and related chemical tracers 1. Model description, J. Geophys. Res., 103, 28265–28289, 1998.

Calvert, J. G., Atkinson, R., Kerr, J. A., Madronich, S., Moortgat, G. K., Wallington, T. J., and Yarwood, G.: The Mechanisms of Atmospheric Oxidation of the Alkenes, Oxford University Press, Oxford, 2000

Carslaw, N., Creasey, D. J., Heard, D. E., Lewis, A. C., McQuaid, J. B., Pilling, M. J., Monks, P. S., Bandy, B. J., and Penkett, S. A.: Modeling OH, HO_2, and RO_2 radicals in the marine boundary layer – 1. Model construction and comparison with field measurements, J. Geophys. Res., 104, 30241–30255, 1999a.

Carslaw, N., Jacobs, P. J., and Pilling, M. J.: Modeling OH, HO_2, and RO_2 radicals in the marine boundary layer 2. Mechanism reduction and uncertainty analysis, J. Geophys. Res., 104, 30257–30273, 1999b.

Carslaw, N., Creasey, D. J., Harrison, D., Heard, D. E., Hunter, M. C., Jacobs, P. J., Jenkin, M. E., Lee, J. D., Lewis, A. C., Pilling, M. J., Saunders, S. M., and Seakins, P. W.: OH and HO_2 radical chemistry in a forested region of north-western Greece, Atmos. Environ., 35, 4725–4737, 2001.

Carslaw, N., Creasey, D. J., Heard, D. E., Jacobs, P. J., Lee, J. D., Lewis, A. C., McQuaid, J. B., Pilling, M. J., Bauguitte, S., Penkett, S. A., Monks, P. S., and Salisbury, G.: Eastern Atlantic Spring Experiment 1997 (EASE97) – 2. Comparisons of model concentrations of OH, HO2, and RO2 with measurements, J. Geophys. Res., 107, D14, 4190, 2002.

Carter, W. P. L.: Development of a condensed SAPRC-07 chemical mechanism, Atmos. Environ., 44, 5336–5345, 2010.

Cotte, H.: Développement d'une technique spectroradiométrique pour la détermination expérimentale des fréquences de photolyse troposphérique: Application au bilan photostationnaire de radicaux libres des campagnes FieldVOC., U.F.R de Chimie, Université Paris VII – Denis Diderot, Paris, 52–118, 1995.

Creasey, D. J., Heard, D. E., and Lee, J. D.: OH and HO_2 measurements in a forested region of north-western Greece, Atmos. Environ., 35, 4713–4724, 2001.

Creasey, D. J., Heard, D. E., and Lee, J. D.: Eastern Atlantic Spring Experiment 1997 (EASE97) 1. Measurements of OH and HO_2 concentrations at Mace Head, Ireland, J. Geophys. Res., 107, D10, 4091, 2002.

Derwent, R. G.: The influence of human activities on the distribution of hydroxyl radicals in the troposphere, Philos. T. R. Soc. A, 354, 501–531, 1996.

Detournay, A., Sauvage, S., Locoge, N., Gaudion, V., Leonardis, T., Fronval, I., Kaluzny, P., and Galloo, J. C.: Development of a sampling method for the simultaneous monitoring of straight-chain alkanes, straight-chain saturated carbonyl compounds and monoterpenes in remote areas, J. Environ. Monitor., 13, 983–990, 2011.

Donahue, N. M., Kroll, J. H., Anderson, J. G., and Demerjian, K. L.: Direct observation of OH production from the ozonolysis of olefins, Geophys. Res. Lett., 25, 59–62, 1998.

Dunlea, E. J. and Ravishankara, A. R.: Measurement of the rate coefficient for the reaction of O((1)D) with H(2)O and re-evaluation of the atmospheric OH production rate, Phys. Chem. Chem. Phys., 6, 3333–3340, 2004a.

Dunlea, E. J. and Ravishankara, A. R.: Kinetic studies of the reactions of O((1)D) with several atmospheric molecules, Phys. Chem. Chem. Phys., 6, 2152–2161, 2004b.

Dusanter, S., Vimal, D., Stevens, P. S., Volkamer, R., Molina, L. T., Baker, A., Meinardi, S., Blake, D., Sheehy, P., Merten, A., Zhang, R., Zheng, J., Fortner, E. C., Junkermann, W., Dubey, M., Rahn, T., Eichinger, B., Lewandowski, P., Prueger, J., and Holder, H.: Measurements of OH and HO2 concentrations during the MCMA-2006 field campaign – Part 2: Model comparison and radical budget, Atmos. Chem. Phys., 9, 6655–6675, doi:10.5194/acp-9-6655-2009, 2009.

Elshorbany, Y. F., Kurtenbach, R., Wiesen, P., Lissi, E., Rubio, M., Villena, G., Gramsch, E., Rickard, A. R., Pilling, M. J., and Kleffmann, J.: Oxidation capacity of the city air of Santiago, Chile, Atmos. Chem. Phys., 9, 2257–2273, doi:10.5194/acp-9-2257-2009, 2009.

Eisele, F. L. and Tanner, D. J.: Ion-assisted tropospheric OH measurements, J. Geophys. Res., 96, 9295–9308, 1991.

Eisele, F. L., Mount, G. H., Tanner, D., Jefferson, A., Shetter, R., Harder, J. W., and Williams, E. J.: Understanding the production and interconversion of the hydroxyl radical during the Tropospheric OH Photochemistry Experiment, J. Geophys. Res., 102, 6457–6465, 1997.

Emmerson, K. M., Carslaw, N., Carpenter, L. J., Heard, D. E., Lee, J. D., and Pilling, M. J.: Urban atmospheric chemistry during the PUMA campaign 1: Comparison of modelled OH and HO_2 concentrations with measurements, J. Atmos. Chem., 52, 143–164, 2005a.

Emmerson, K. M., Carslaw, N., and Pilling, M. J.: Urban atmospheric chemistry during the PUMA campaign 2: Radical budgets for OH, HO_2 and RO_2, J. Atmos. Chem., 52, 165–183, 2005b.

Emmerson, K. M., Carslaw, N., Carslaw, D. C., Lee, J. D., McFiggans, G., Bloss, W. J., Gravestock, T., Heard, D. E., Hopkins, J., Ingham, T., Pilling, M. J., Smith, S. C., Jacob, M., and Monks, P. S.: Free radical modelling studies during the UK TORCH Campaign in Summer 2003, Atmos. Chem. Phys., 7, 167–181, doi:10.5194/acp-7-167-2007, 2007.

Finlayson-Pitts, B. J. and Pitts, J. N.: Chemistry of the upper and lower atmosphere, Academic Press, San Diego, 2000.

Freutel, F., Schneider, J., Drewnick, F., von der Weiden-Reinmüller, S.-L., Crippa, M., Prévôt, A. S. H., Baltensperger, U., Poulain, L., Wiedensohler, A., Sciare, J., Sarda-Estève, R., Burkhart, J. F., Eckhardt, S., Stohl, A., Gros, V., Colomb, A., Michoud, V., Doussin, J. F., Borbon, A., Haeffelin, M., Morille, Y., Beekmann, M., and Borrmann, S.: Aerosol particle measurements at three stationary sites in the megacity of Paris during summer 2009: meteorology and air mass origin dominate aerosol particle composition and size distribution, Atmos. Chem. Phys. Discuss., 12, 22199–22268, doi:10.5194/acpd-12-22199-2012, 2012.

Fuchs, H., Bohn, B., Hofzumahaus, A., Holland, F., Lu, K. D., Nehr, S., Rohrer, F., and Wahner, A.: Detection of HO_2 by laser-induced fluorescence: calibration and interferences from RO_2 radicals, Atmos. Meas. Tech., 4, 1209–1225, doi:10.5194/amt-4-1209-2011, 2011.

George, L. A., Hard, T. M., and O'Brien, R. J.: Measurement of free radicals OH and HO_2 in Los Angeles smog, J. Geophys. Res., 104, 11643–11655, 1999.

Geyer, A., Bachmann, K., Hofzumahaus, A., Holland, F., Konrad, S., Klupfel, T., Patz, H. W., Perner, D., Mihelcic, D., Schafer, H. J., Volz-Thomas, A., and Platt, U.: Nighttime formation of peroxy and hydroxyl radicals during the BERLIOZ campaign: Observations and modeling studies, J. Geophys. Res.-Atmos., 108, doi:10.1029/2001jd000656, 2003.

Gros, V., Bonsang, B., and Sarda Esteve, R.: Atmospheric carbon monoxide "in situ" monitoring by automatic gas chromatography, Chemosphere – Global Change Science, 1, 153–161, 1999.

Haeffelin, M., Barthès, L., Bock, O., Boitel, C., Bony, S., Bouniol, D., Chepfer, H., Chiriaco, M., Cuesta, J., Delanoë, J., Drobinski, P., Dufresne, J.-L., Flamant, C., Grall, M., Hodzic, A., Hourdin, F., Lapouge, F., Lemaître, Y., Mathieu, A., Morille, Y., Naud, C., Noël, V., O'Hirok, W., Pelon, J., Pietras, C., Protat, A., Romand, B., Scialom, G., and Vautard, R.: SIRTA, a ground-based atmospheric observatory for cloud and aerosol research, Ann. Geophys., 23, 253–275, doi:10.5194/angeo-23-253-2005, 2005.

Haeffelin, M., Angelini, F., Morille, Y., Martucci, G., Frey, S., Gobbi, G.-P., Lolli, S., O'Dowd, C. D., Sauvage, L., Xueref-Rémy, I., Wastine, B., Feist, D., : Evaluation of mixing height retrievals from automatic profiling lidars and ceilometers in view of future integrated networks in Europe, Bound.-Lay. Meteorol., 143, 49–75, 2011.

Hasel, M., Kottmeier, C., Corsmeier, U., and Wieser, A.: Airborne measurements of turbulent trace gas fluxes and analysis of eddy structure in the convective boundary layer over complex terrain, Atmos. Res., 74, 381–402, 2005.

Heard, D. E. and Pilling, M. J.: Measurement of OH and HO_2 in the troposphere, Chem. Rev., 103, 5163–5198, 2003.

Hofzumahaus, A., Rohrer, F., Lu, K. D., Bohn, B., Brauers, T., Chang, C. C., Fuchs, H., Holland, F., Kita, K., Kondo, Y., Li, X., Lou, S. R., Shao, M., Zeng, L. M., Wahner, A., and Zhang, Y. H.: Amplified Trace Gas Removal in the Troposphere, Science, 324, 1702–1704, 2009.

Holland, F., Hofzumahaus, A., Schafer, R., Kraus, A., and Patz, H. W.: Measurements of OH and HO_2 radical concentrations and photolysis frequencies during BERLIOZ, J. Geophys. Res., 108, D4, 8246, 2003.

Jenkin, M. E., Saunders, S. M., Wagner, V., and Pilling, M. J.: Protocol for the development of the Master Chemical Mechanism, MCM v3 (Part B): tropospheric degradation of aromatic volatile organic compounds, Atmos. Chem. Phys., 3, 181–193, doi:10.5194/acp-3-181-2003, 2003.

Kanaya, Y., Matsumoto, J., Kato, S., and Akimoto, H.: Behavior of OH and HO2 radicals during the Observations at a Remote Island of Okinawa (ORION99) field campaign 2. Comparison between observations and calculations, J. Geophys. Res., 106, 24209–24223, 2001.

Kanaya, Y., Cao, R. Q., Akimoto, H., Fukuda, M., Komazaki, Y., Yokouchi, Y., Koike, M., Tanimoto, H., Takegawa, N., and Kondo, Y.: Urban photochemistry in central Tokyo: 1. Observed and modeled OH and HO_2 radical concentrations during the winter and summer of 2004, J. Geophys. Res., 112, D21312, doi:10.1029/2007JD008670, 2007.

Kanaya, Y., Hofzumahaus, A., Dorn, H.-P., Brauers, T., Fuchs, H., Holland, F., Rohrer, F., Bohn, B., Tillmann, R., Wegener, R., Wahner, A., Kajii, Y., Miyamoto, K., Nishida, S., Watanabe, K., Yoshino, A., Kubistin, D., Martinez, M., Rudolf, M., Harder, H., Berresheim, H., Elste, T., Plass-Dülmer, C., Stange, G., Kleffmann, J., Elshorbany, Y., and Schurath, U.: Comparisons of observed and modeled OH and HO_2 concentrations during the ambient measurement period of the HOxComp field campaign, Atmos. Chem. Phys., 12, 2567–2585, doi:10.5194/acp-12-2567-

2012, 2012.

Kato, S., Sato, T., and Kajii, Y.: A method to estimate the contribution of unidentified VOCs to OH reactivity, Atmos. Environ., 45, 5531–5539, 2011.

Kleffmann, J.: Daytime sources of nitrous acid (HONO) in the atmospheric boundary layer, Chemphyschem, 8, 1137–1144, 2007.

Kleffmann, J., Gavriloaiei, T., Hofzumahaus, A., Holland, F., Koppmann, R., Rupp, L., Schlosser, E., Siese, M., and Wahner, A.: Daytime formation of nitrous acid: A major source of OH radicals in a forest, Geophys. Res. Lett., 32, L05818, doi:10.1029/2005GL022524, 2005.

Kukui, A., Ancellet, G., and Le Bras, G.: Chemical ionisation mass spectrometer for measurements of OH and Peroxy radical concentrations in moderately polluted atmospheres, J. Atmos. Chem., 61, 133–154, 2008.

Levy, H.: Photochemistry of the lower troposphere, Planet. Space Sci, 20, 919–935, 1972.

Liu, Z., Wang, Y., Gu, D., Zhao, C., Huey, L. G., Stickel, R., Liao, J., Shao, M., Zhu, T., Zeng, L., Amoroso, A., Costabile, F., Chang, C.-C., and Liu, S.-C.: Summertime photochemistry during CAREBeijing-2007: RO_x budgets and O_3 formation, Atmos. Chem. Phys. Discuss., 12, 4679–4717, doi:10.5194/acpd-12-4679-2012, 2012.

Lu, K. D., Rohrer, F., Holland, F., Fuchs, H., Bohn, B., Brauers, T., Chang, C. C., Häseler, R., Hu, M., Kita, K., Kondo, Y., Li, X., Lou, S. R., Nehr, S., Shao, M., Zeng, L. M., Wahner, A., Zhang, Y. H., and Hofzumahaus, A.: Observation and modelling of OH and HO_2 concentrations in the Pearl River Delta 2006: a missing OH source in a VOC rich atmosphere, Atmos. Chem. Phys., 12, 1541–1569, 2012, http://www.atmos-chem-phys.net/12/1541/2012/.

Madronich, S., McKenzie, R. L., Bjorn, L. O., and Caldwell, M. M.: Changes in biologically active ultraviolet radiation reaching the Earth's surface, J. Photoch. Photobio. A, 46, 5–19, 1998.

Mao, J., Ren, X., Zhang, L., Van Duin, D. M., Cohen, R. C., Park, J.-H., Goldstein, A. H., Paulot, F., Beaver, M. R., Crounse, J. D., Wennberg, P. O., DiGangi, J. P., Henry, S. B., Keutsch, F. N., Park, C., Schade, G. W., Wolfe, G. M., Thornton, J. A., and Brune, W. H.: Insights into hydroxyl measurements and atmospheric oxidation in a California forest, Atmos. Chem. Phys., 12, 8009–8020, doi:10.5194/acp-12-8009-2012, 2012.

Martinez, M., Harder, H., Kovacs, T. A., Simpas, J. B., Bassis, J., Lesher, R., Brune, W. H., Frost, G. J., Williams, E. J., Stroud, C. A., Jobson, B. T., Roberts, J. M., Hall, S. R., Shetter, R. E., Wert, B., Fried, A., Alicke, B., Stutz, J., Young, V. L., White, A. B., and Zamora, R. J.: OH and HO_2 concentrations, sources, and loss rates during the Southern Oxidants Study in Nashville, Tennessee, summer 1999, J. Geophys. Res., 108, D19, 4617, 2003.

McKenzie, R. L., Aucamp, P. J., Bais, A. F., Bjorn, L. O., and Ilyas, M.: Changes in biologically-active ultraviolet radiation reaching the Earth's surface, Photoch. Photobio. Sci., 6, 218–231, 2007.

Mihelcic, D., Holland, F., Hofzumahaus, A., Hoppe, L., Konrad, S., Musgen, P., Patz, H. W., Schafer, H. J., Schmitz, T., Volz-Thomas, A., Bachmann, K., Schlomski, S., Platt, U., Geyer, A., Alicke, B., and Moortgat, G. K.: Peroxy radicals during BERLIOZ at Pabstthum: Measurements, radical budgets and ozone production, J. Geophys. Res., 108, D4, 8254, 2003.

Mount, G. H., and Williams, E. J.: An overview of the tropospheric OH photochemistry experiment, Fritz Peak Idaho Hill, Colorado, Fall 1993, J. Geophys. Res., 102, 6171–6186, 1997.

Nielsen, T., Hansen, A. M., and Thomsen, E. L.: A convenient method for preparation of pure standards of peroxyacetyl nitrate for atmospheric analyses, Atmos. Environ., 16, 2447–2450, 1982.

Pietras, C., Boitel, C., Dupont, J. C., Haeffelin, M., Lapouge, F., Morille, Y., Noel, V., and Romand, B.: SIRTA, a multi-sensor platform for clouds and aerosols characterization in the atmosphere: infrastructure, objective and prospective - art. no. 67501A, in: Lidar Technologies, Techniques, and Measurements for Atmospheric Remote Sensing Iii, P. Soc. Photo-Opt. Inst., A7501–A7501, 2007.

Reiner, T., Hanke, M., and Arnold, F.: Atmospheric peroxy radical measurements by ion molecule reaction mass spectrometry: A novel analytical method using amplifying chemical conversion to sulfuric acid, J. Geophys. Res., 102, 1311–1326, 1997.

Ren, X. R., Harder, H., Martinez, M., Lesher, R. L., Oliger, A., Shirley, T., Adams, J., Simpas, J. B., and Brune, W. H.: HO_x concentrations and OH reactivity observations in New York City during PMTACS-NY2001, Atmos. Environ., 37, 3627–3637, 2003a.

Ren, X. R., Harder, H., Martinez, M., Lesher, R. L., Oliger, A., Simpas, J. B., Brune, W. H., Schwab, J. J., Demerjian, K. L., He, Y., Zhou, X. L., and Gao, H. G.: OH and HO2 chemistry in the urban atmosphere of New York City, Atmos. Environ., 37, 3639–3651, 2003b.

Ren, X. R., Brune, W. H., Oliger, A., Metcalf, A. R., Simpas, J. B., Shirley, T., Schwab, J. J., Bai, C. H., Roychowdhury, U., Li, Y. Q., Cai, C. X., Demerjian, K. L., He, Y., Zhou, X. L., Gao, H. L., and Hou, J.: OH, HO_2, and OH reactivity during the PMTACS-NY Whiteface Mountain 2002 campaign: Observations and model comparison, J. Geophys. Res., 111, D10S03, doi:10.1029/2005JD006126, 2006.

Ren, X. R., Olson, J. R., Crawford, J. H., Brune, W. H., Mao, J. Q., Long, R. B., Chen, Z., Chen, G., Avery, M. A., Sachse, G. W., Barrick, J. D., Diskin, G. S., Huey, L. G., Fried, A., Cohen, R. C., Heikes, B., Wennberg, P. O., Singh, H. B., Blake, D. R., and Shetter, R. E.: HO(x) chemistry during INTEX-A 2004: Observation, model calculation, and comparison with previous studies, J. Geophys. Res., 113, D05310, doi:10.1029/2007JD009166, 2008.

Salisbury, G., Rickard, A. R., Monks, P. S., Allan, B. J., Bauguitte, S., Penkett, S. A., Carslaw, N., Lewis, A. C., Creasey, D. J., Heard, D. E., Jacobs, P. J., and Lee, J. D.: Production of peroxy radicals at night via reactions of ozone and the nitrate radical in the marine boundary layer, J. Geophys. Res.-Atmos., 106, 12669–12687, doi:10.1029/2000jd900754, 2001.

Saunders, S. M., Jenkin, M. E., Derwent, R. G., and Pilling, M. J.: World Wide Web site of a Master Chemical Mechanism (MCM) for use in tropospheric chemistry models, Atmos. Environ., 31, 1249–1249, 1997.

Saunders, S. M., Jenkin, M. E., Derwent, R. G., and Pilling, M. J.: Protocol for the development of the Master Chemical Mechanism, MCM v3 (Part A): tropospheric degradation of non-aromatic volatile organic compounds, Atmos. Chem. Phys., 3, 161–180, doi:10.5194/acp-3-161-2003, 2003.

Shirley, T. R., Brune, W. H., Ren, X., Mao, J., Lesher, R., Cardenas, B., Volkamer, R., Molina, L. T., Molina, M. J., Lamb, B., Velasco, E., Jobson, T., and Alexander, M.: Atmospheric oxidation in the Mexico City Metropolitan Area (MCMA) during April 2003, Atmos. Chem. Phys., 6, 2753–2765, doi:10.5194/acp-6-

2753-2006, 2006.

Smith, S. C., Lee, J. D., Bloss, W. J., Johnson, G. P., Ingham, T., and Heard, D. E.: Concentrations of OH and HO_2 radicals during NAMBLEX: measurements and steady state analysis, Atmos. Chem. Phys., 6, 1435–1453, doi:10.5194/acp-6-1435-2006, 2006.

Sommariva, R., Bloss, W. J., Brough, N., Carslaw, N., Flynn, M., Haggerstone, A.-L., Heard, D. E., Hopkins, J. R., Lee, J. D., Lewis, A. C., McFiggans, G., Monks, P. S., Penkett, S. A., Pilling, M. J., Plane, J. M. C., Read, K. A., Saiz-Lopez, A., Rickard, A. R., and Williams, P. I.: OH and HO_2 chemistry during NAMBLEX: roles of oxygenates, halogen oxides and heterogeneous uptake, Atmos. Chem. Phys., 6, 1135–1153, doi:10.5194/acp-6-1135-2006, 2006.

Stockwell, W. R., Kirchner, F., Kuhn, M., and Seefeld, S.: A new mechanism for regional atmospheric chemistry modeling, J. Geophys. Res., 102, 25847–25879, 1997.

Stohl, A., Forster, C., Frank, A., Seibert, P., and Wotawa, G.: Technical note: The Lagrangian particle dispersion model FLEXPART version 6.2, Atmos. Chem. Phys., 5, 2461–2474, doi:10.5194/acp-5-2461-2005, 2005.

Tan, D., Faloona, I., Simpas, J. B., Brune, W., Shepson, P. B., Couch, T. L., Sumner, A. L., Carroll, M. A., Thornberry, T., Apel, E., Riemer, D., and Stockwell, W.: HO_x budgets in a deciduous forest: Results from the PROPHET summer 1998 campaign, J. Geophys. Res., 106, 24407–24427, 2001.

Tanner, D. J., Jefferson, A., and Eisele, F. L.: Selected ion chemical ionization mass spectrometric measurement of OH, J. Geophys. Res., 102, 6415–6425, 1997.

Verwer, J. G. and Vanloon, M.: An Evaluation of Explicit Pseudo-Steady-State Approximation Schemes for Stiff Ode Systems from Chemical-Kinetics, J. Comput. Phys., 113, 347–352, 1994.

Verwer, J. G., Blom, J. G., VanLoon, M., and Spee, E. J.: A comparison of stiff ODE solvers for atmospheric chemistry problems, Atmos. Environ., 30, 49–58, 1996.

Volkamer, R., Sheehy, P., Molina, L. T., and Molina, M. J.: Oxidative capacity of the Mexico City atmosphere – Part 1: A radical source perspective, Atmos. Chem. Phys., 10, 6969–6991, doi:10.5194/acp-10-6969-2010, 2010.

Wang, J., Doussin, J. F., Perrier, S., Perraudin, E., Katrib, Y., Pangui, E., and Picquet-Varrault, B.: Design of a new multi-phase experimental simulation chamber for atmospheric photosmog, aerosol and cloud chemistry research, Atmos. Meas. Tech., 4, 2465–2494, doi:10.5194/amt-4-2465-2011, 2011.

Webb, R., Stromberg, I. M., Li, H., and Barttlett, L. M.: Airborne spectral measurements of surface reflectivity at ultraviolet and visible wavelengths, J. Geophys. Res., 105, 4945–4948, 2000.